# MASARYK UNIVERSITY

**FACULTY OF SCIENCE** 

# Anisotropic linear dielectric response of cubic crystals exhibiting achiral symmetry

Master's Thesis

BEÁTA HRONCOVÁ

Brno, Spring 2025

# MASARYK UNIVERSITY

**FACULTY OF SCIENCE** 

# Anisotropic linear dielectric response of cubic crystals exhibiting achiral symmetry

Master's Thesis

BEÁTA HRONCOVÁ

Advisor: Mgr. Daniel Franta, Ph.D.

Department of Theoretical Physics and Astrophysics

Brno, Spring 2025



# **Bibliographic record**

Author: Beáta Hroncová

Faculty of Science Masaryk University

Department of Theoretical Physics and Astrophysics

Title of Thesis: Anisotropic linear dielectric response of cubic crystals exhibiting

achiral symmetry

**Degree Programme:** Physics

**Field of Study:** Theoretical physics

**Supervisor:** Mgr. Daniel Franta, Ph.D.

**Academic Year:** 2024/2025

Number of Pages: 50

**Keywords:** optical anisotropy, cubic crystals, dielectric response, spatial dis-

persion

## **Abstract**

Assuming a local response is a commonly used approximation in calculating the dielectric tensor. Terms that appear beyond this approximation are collectively called spatial dispersion. These terms depend on the wavevector of the propagating light. We focus on the quadratic term, specifically in achiral cubic crystals where the symmetry forbids the linear term. The fact that cubic crystals are isotropic within the local response approximation allows us to assess the weak spatial dispersion.

We analyzed Si crystals with (001), (011), and (111) surface orientations, and  $CaF_2$  crystal with (111) orientation. We fitted the acquired linear birefringence data to obtain the spectral functions of the dielectric tensor.

We also measured the azimuthal angle dependence of linear birefringence at oblique angles of incidence for a single wavelength. The results for  $CaF_2$  qualitatively agree with published literature [1]. The results for Si exhibit strong dependence on the thickness of the native oxide layer. We were able to fit the acquired linear retardance using the spectral function from the normal incidence measurement. We are not aware of any publication the Si results could be compared against.



MASARYKOVA UNIVERZITA PŘÍRODOVĚDECKÁ FAKULTA

KOTLÁŘSKÁ 2, 611 37 BRNO

IČ: 00216224 DIČ: CZ00216224

# ZADÁNÍ DIPLOMOVÉ PRÁCE

Akademický rok: 2024/2025

Ústav:	Ústav teoretické fyziky a astrofyziky		
Studentka:	Bc. Beáta Hroncová		
Program:	Fyzika		
Specializace:	Teoretická fyzika		

Ředitel ústavu PřF MU Vám ve smyslu Studijního a zkušebního řádu MU určuje diplomovou práci s názvem:

Název práce:	Anizotropní lineární dielektrická odezva kubických krystalů s nechirální symetrií
Název práce anglicky:	Anisotropic linear dielectric response of cubic crystals exhibiting achiral symmetry
Jazyk práce:	angličtina

#### Oficiální zadání:

Je všeobecně známé, že pokud se zanedbají efekty spojené s prostorovou disperzí, kubické krystaly vykazují izotropní lineární dielektrickou odezvu. Ovšem v případě, že prostorová disperze se nezanedbá, kubické krystaly vykazují dvojlom, ať už cirkulární (optickou aktivitu) a nebo lineární (slabou anizotropii). Tyto slabé efekty závisí na směru a velikosti vlnového vektoru, kterým se světlo v kubickém krystalu šíří. Optická aktivita je v kubických krystalech spojena s chirální symetrií, a v prvním přiblížení závisí lineárně na velikosti vlnového vektoru. V případě, že krystal nevykazuje chirální symetrii, prostorová disperze nevykazuje komponenty s lichou mocninnou závislostí na velikosti vlnového vektoru, ale pouze komponenty se sudou mocninnou závislostí. Prostorová disperze má původ v konečném okolí studovaného bodu, a proto jak bylo ukázáno v práci [1] v chirálních prostředí závislost není přesně lineární, ale mírně odlišná. Proto bylo nutné vytvořit disperzní model s komponenty závislosti na velikosti vlnového vektoru vyššího řádu než lineární. Tento disperzní model byl formulovaný na základě řešení klasických pohybových rovnic a vede k modelu opticky aktivních harmonických oscilátorů. Jak bylo ukázáno v práci [2] kubický člen v deformačním tenzoru izotropního modelu posouvá rezonanční frekvenci podélné komponenty odezvové funkce vzhledem k příčným komponentám této funkce v členech, které jsou lineární na vlnovém vektoru. Je logické, že v případě kubických krystalů s nechirální symetrií kubický člen deformačního tenzoru bude manipulovat s rezonančními frekvencemi všech komponent odezvové funkce, tedy i s rezonančními frekvencemi odpovídající příčným módům šíření světla v anizotropním prostředí. Tento efekt ovšem bude pozorovatelný pouze podél os s dvojčetnou symetrií (v kubickém krystalu podél směru (110)) a nebude pozorovatelný podél os s vícečetnou symetrií (v kubickém krystalu podél směrů (100) a (111)).

Předmětem práce bude teoretické studium dielektrické odezvy kubických krystalů nevykazující chirální symetrii. V rámci teoretické studie bude několik úkolů.

- 1. V prvním kroku bude nutné formulovat tenzorový počet zahrnující sudé komponenty rozvoje závislosti na vlnovém vektoru.
- 2. V rámci tohoto vektorového počtu zobecnit disperzní model opticky aktivních harmonických oscilátorů, tak aby byl schopen popsat dvojlom ve studovaných prostředích.
- 3. Výsledky srovnat s experimentálními daty [3] naměřenými pomocí zobecněné elipsometrie na krystalických křemíkových destičkách s orientací povrchu (110) v prošlém i odraženém světle.
- [1] Bakalářská práce Beáty Hroncové, Charakterizace opticky aktivních kapalin, PřF MU Brno 2022.
- [2] Franta D., Vohánka J., Constitutive equations describing optical activity in theory of dispersion, Journal of the Optical Society of America B 38 (2021) 553-561; Franta D., Symmetry of Linear Dielectric Response Tensors: Dispersion Models Fulfilling Three Fundamental Conditions, Journal of Applied Physics 127 (2020) 223101.
- [3] S. Bian, R. Ossikovski, A. Canillas, G. Jellison, and O. Arteaga, "Spatial dispersion in silicon", Phys. Rev. B, vol. 109, p. 035 201, 3, 2024, doi: 10.1103/PhysRevB.109.035201

Vedoucí práce:	Mgr. Daniel Franta, Ph.D.
Konzultant:	Mgr. Jiří Vohánka, Ph.D.
Datum zadání práce:	30. 11. 2022
V Brně dne:	6. 5. 2025

Bc. Beáta Hroncová, 5. 5. 2025 Mgr. Daniel Franta, Ph.D., 5. 5. 2025 Mgr. Dušan Hemzal, Ph.D., 5. 5. 2025

# Acknowledgements Týmto by som chcela poďakovať vedúcemu práce Mgr. Danielovi Frantovi, Ph.D. a konzultantovi Mgr. Jiřímu Vohánkovi, Ph.D. Špeciálna vďaka patrí spolupracujúcim: Orol Arteaga, Subiao Bian, prof. Razvigor Ossikovski, ďalej Bibke, Petrovi, rodičom, ...

# **Declaration**

Hereby I declare that this paper is my original authorial work, which I have worked out on my own. All sources, references, and literature used or excerpted during elaboration of this work are properly cited and listed in complete reference to the due source.

Beáta Hroncová

# **Contents**

Int	roduc	tion	1
1	1.1 1.2 1.3 1.4 1.5	Electromagnetic field	4
2	Mod 2.1 2.2 2.3 2.4	Symmetries of the dielectric tensor Real crystal corrections  2.2.1 Boundary conditions Dispersion model Berreman's formalism  2.4.1 Coherent multiple reflections  2.4.2 Incoherent multiple reflections  2.4.3 No multiple reflections	17 17 19 19 23 25 25 28 30
3	3.1 3.2 3.3	Perimental methods  Mueller matrices	31 33 35 37
5 Bil	4.2 Cond	Spatial analysis	39 45 47

## Introduction

In natural materials, the wavelength of a probing electromagnetic wave is often assumed to be much larger than interatomic distances [2]. This approximation greatly simplifies calculations, but even on common materials such as silicon, we can observe small deviations from the expected symmetries [3, 4]. Terms that appear beyond this approximation are collectively called spatial dispersion.

A concrete example is what happened to the 157 nm optical litography, where the discovery of spatial dispersion effects in  $CaF_2$  and  $BaF_2$  led to a major effort to correct the resulting aberations [1, 5].

This thesis focuses on the theory of spatial dispersion and its application to polarimetric measurements on silicon and CaF<sub>2</sub>.

The first chapter serves as a general introduction into the theory of linear optical response. We go step by step through the fundamental derivation whilst staying away from the local response approximation. This approach leads us to a wavevector dependent response. One could do an one-line *ad hoc* series expansion of the dielectric response that would lead us to the same result. We, however, like to provide a little bit of insight into the nature of spatial dispersion.

In the second chapter we take a closer look at cubic crystals, speciffically the achiral ones, which do not exhibit any gyrotropy. We translate the symmetries of these systems into the symmetries of the dielectric response. We porpose two simple spatial dispersion models in the transparent spectral range. We also outline how to modify traditional computation methods so that they account for spatial dispersion.

The third chapter provides an overview of the experimental methods used. We also describe the samples which were used in this study.

The fourth chapter concerns the experimental results and is divided into two parts. In the first part, we study the spectral dependence of the dielectric tensor and evaluate the validity of the proposed models. In the second part, we analyze the angular dependence of the linear birefringence stemming from spatial dispersion.

# 1 Dielectric response with spatial dispersion

The main objective of this chapter is to give a basic understanding of the linear dielectric response of a material to external electromagnetic field. We recall the frequently used optical constants and revise them in order to include small anisotropic terms which are typically neglected. The beginning of this chapter gives a basic definition of the electromagnetic susceptibility. The approach begins with a general description and incrementally incorporates more specific assumptions, leading to the linear optical response of semiconductors.

# 1.1 Electromagnetic field

The electromagnetic field is completely described by the electric field E and magnetic induction B. It can be equivalently described in terms of the scalar  $\Phi$  and vector potential A which are linked to the fields by equations

$$E(\mathbf{r},t) = -\nabla \Phi(\mathbf{r},t) - \frac{\partial}{\partial t} A(\mathbf{r},t), \qquad (1.1a)$$

$$B(r,t) = \nabla \times A(r,t). \tag{1.1b}$$

The potentials are not unique. A transformation by a scalar field  $\Lambda$  can be introduced as

$$\Phi \to \Phi - \partial_t \Lambda$$
 and  $A \to A + \nabla \Lambda$ , (1.2)

which does not change any measurable quantities, *i. e.* it preserves equations (1.1). In the following we will use  $\Lambda$  such that  $\nabla \cdot A = 0$ . This condition does not determine  $\Lambda$  unambigously. Even now we can still add another scalar function  $\tilde{\Lambda}$  that satisfies the Laplace equation  $\Delta \tilde{\Lambda}$ . This time we choose  $\tilde{\Lambda}$  for which  $\Phi = 0$ . In other words, we will use the *Coulomb gauge*.

Inside a material medium, however, particles can behave like electric dipoles or create magnetic dipole moments. This results in new contributions to the electromagnetic fields which are referred to as dielectric polarization P and magnetization M, respectively. When working with matter, it is convenient to define auxiliary fields called electric induction D and magnetic field H by subtracting the material response

$$D(\mathbf{r},t) = \epsilon_0 E(\mathbf{r},t) + P(\mathbf{r},t), \tag{1.3a}$$

$$H(\mathbf{r},t) = \frac{1}{\mu_0}B(\mathbf{r},t) - M(\mathbf{r},t). \tag{1.3b}$$

The new fields simplify Maxwell's equations in a way that only free charges and free currents remain as sources. The remaining task is then to find a relation between the auxiliary and the actual fields.

Most of non-magnetic materials show no or only a negligible magnetization at optical frequencies, and hence we will put  $H = B/\mu_0$ . In fact, in an infinite medium there is, in general, no clear boundary between polarization current and magnetization current. This issue was thoroughy discussed by Landau *et. al.* in [6].

# 1.2 Minimal coupling

In optical experiments, the probing light has a very low electromagnetic field compared to fields bewteen particles of matter [6]. We will treat the external fields as a time dependent perturbation. The total Hamiltonian of the system of matter particles and the field can be divided into three parts

$$\hat{\mathcal{H}} = \hat{\mathcal{H}}_{M,0} + \hat{\mathcal{H}}_{F,0} + \hat{\mathcal{H}}_{int},\tag{1.4}$$

where  $\hat{\mathcal{H}}_0 = \hat{\mathcal{H}}_{F,0} + \hat{\mathcal{H}}_{M,0}$  is the Hamiltonian of a non-interacting system and  $\hat{\mathcal{H}}_{int}$  contains the interaction of particles with the electromagnetic field. Note that the Hamiltonian  $\hat{\mathcal{H}}$  acts on a Hilbert space  $\mathscr{H}_M \otimes \mathscr{H}_F$  (everything matter related will carry subscript "M" and electromagnetic field related will be subscripted with "F"). The action of  $\hat{\mathcal{H}}_{M,0}$  on the subspace  $\mathscr{H}_F$  is trivial (identity). The same holds for  $\hat{\mathcal{H}}_{F,0}$  acting on  $\mathscr{H}_M$ .

To derive the interaction operator we are going to consider *minimal coupling* of a particle to the electromagnetic field [7]. It describes the interaction term by replacing the momentum operator with the canonical momentum,  $\hat{p} \rightarrow \hat{p} - q\hat{A}$ , which is the conjugate variable of position. The symbol q denotes the charge of the particle. From this we can easily find the interaction term of the matter Hamiltonian

$$\hat{\mathcal{H}}_{M,0} + \hat{\mathcal{H}}_{int} = \sum_{n} \frac{\hat{p}_{n}^{2}}{2m_{n}} + \hat{V} + \hat{\mathcal{H}}_{int} 
= \sum_{n} \frac{1}{2m_{n}} (\hat{p}_{n} - q_{n}\hat{A})^{2} + \hat{V},$$
(1.5)

where  $\hat{V}$  includes all interactions between particles and depends only on their positions  $r_n$ . Using the Coulomb gauge<sup>1</sup> we get

$$\hat{\mathcal{H}}_{int} = \sum_{n} \frac{1}{2m_n} \left( \hat{\boldsymbol{p}}_n - q_n \hat{\boldsymbol{A}} \right)^2 - \sum_{n} \frac{\hat{\boldsymbol{p}}_n^2}{2m_n}$$

$$= -\sum_{n} \frac{q_n}{m_n} \hat{\boldsymbol{p}}_n \cdot \hat{\boldsymbol{A}} + \sum_{n} \frac{q_n^2}{2m_n} \hat{\boldsymbol{A}} \cdot \hat{\boldsymbol{A}}$$

$$= -\hat{\boldsymbol{J}} \cdot \hat{\boldsymbol{A}} + \sum_{n} \frac{q_n^2}{2m_n} \hat{\boldsymbol{A}} \cdot \hat{\boldsymbol{A}},$$
(1.6)

<sup>1.</sup> It is straightforward to show that  $\hat{A}$  commutes with  $\hat{p}$  from the Coulomb gauge,  $\nabla \cdot A = 0$ , and the position representation of  $\hat{p} = -i\hbar \nabla$ .

where we have defined the total current operator  $\hat{J} = -\sum_n \frac{q_n}{m_n} \hat{p}_n$ . Using the symmetric Weyl ordering [7], we can also define the *current-density operator* at position r,  $\hat{j}(r)$ , as [8]

$$\hat{\boldsymbol{j}}(r) = -\sum_{n} \frac{q_n}{2m_n} \left[ \hat{\boldsymbol{p}}_n \delta(\boldsymbol{r} - \hat{\boldsymbol{r}}_n) + \delta(\boldsymbol{r} - \hat{\boldsymbol{r}}_n) \hat{\boldsymbol{p}}_n \right]. \tag{1.7}$$

#### 1.3 Kubo formula

In this section, we describe how matter responds to small applied fields. The resulting linear response functions are called Kubo formulae.

Throughout this chapter we will work in the *Heisenberg picture*. This means that quantum state vectors  $|n\rangle$  are constant in time and operators corresponding to observables evolve in time according to the Hamitlonian  $\hat{\mathcal{H}}$  as

$$\hat{\mathcal{O}}(t) = e^{\frac{i}{\hbar}\hat{\mathcal{H}}t}\hat{\mathcal{O}}e^{-\frac{i}{\hbar}\hat{\mathcal{H}}t},\tag{1.8}$$

as the Hamiltonian is the generator of infinitesimal translation in time. Operators without explicit time dependence are thought as evaluated at time t=0 or, equivalently, as operators in *Schrödinger picture*. The exponential of an operator is understood as *Taylor series* of the exponential function.

At finite temperatures, the system does not stay in the ground state but rather tends to a thermodynamic equilibrium. This generally incoherent combination of states is conveniently described by the *density matrix*  $\rho$ . In the absence of interactions  $\hat{\mathcal{H}}_{int}$ ,

$$\hat{\rho}_0 = \frac{1}{z} e^{-\beta(\hat{\mathcal{H}}_0 - \mu \hat{N})}, \quad z = \text{Tr}\left(e^{-\beta(\hat{\mathcal{H}}_0 - \mu \hat{N})}\right), \tag{1.9}$$

where z is called the *grand partition function* [9],  $\hat{N}$  is the particle number operator, and  $\mu$  the chemical potential. The symbol Tr  $(...) = \sum_{n} \langle n | ... | n \rangle$  denotes the trace and is independent of the chosen basis  $\{|n\rangle\}$  of the respective Hilbert space  $\mathscr{H}$ . The factor  $\beta$  is

$$\beta = \frac{1}{k_{\rm B}T} \tag{1.10}$$

with  $k_{\rm B}$  the *Boltzmann constant* and T the thermodynamic temperature.

After slowly switching on the interaction<sup>2</sup>  $\hat{\mathcal{H}}_{int}$ , the system changes its state to a different equilibrium. This change is represented by a small perturbation  $\Delta \rho$  which depends on time,

$$\hat{\rho}(t) = \hat{\rho}_0 + \Delta \hat{\rho}(t). \tag{1.11}$$

<sup>2.</sup> It is important that the interaction is turned on slowly so that the system has time to adapt to the change and stays in thermodynamic equilibrium. Otherwise it would be very cumbersome or even impossible to assign a density matrix to the system and make any predictions [8].

One can derive the time evolution of the operator  $\Delta \hat{\rho}$  by using the equation of motion [8]

 $\Delta \hat{\rho}(t) = \int_{-\infty}^{t} \left[ \hat{\mathcal{H}}_{int}(t'), \hat{\rho}_{0} \right] dt', \qquad (1.12)$ 

where higher order terms, which lead to non-linear response, were already neglected.

Recalling equation (1.3a), we will try to find the polarization field inside a medium as a linear response to the external electromagnetic field<sup>3</sup>. Any observable quantity, in our case the dielectric polarization P, is the expectation value of the corresponding operator [10]

$$\mathbf{P}(\mathbf{r},t) = \langle \hat{\mathbf{P}}(\mathbf{r}) \rangle(t) = \text{Tr} \left[ \hat{\rho}(t) \hat{\mathbf{P}}(\mathbf{r},t) \right], \tag{1.13}$$

where  $\langle ... \rangle$  denotes the statistical mean value prescribed by the second equality. After inserting (1.11) and (1.12) and neglecting higher order terms, we get to the relation

$$\langle \hat{\boldsymbol{P}}(\boldsymbol{r}) \rangle(t) = \langle \hat{\boldsymbol{P}}(\boldsymbol{r}) \rangle_0 - \frac{i}{\hbar} \int_{-\infty}^{\infty} \langle \left[ \hat{\boldsymbol{P}}(\boldsymbol{r}, t), \hat{\mathcal{H}}_{int}(t') \right] \rangle_0 \, \vartheta(t - t') \, dt'. \tag{1.14}$$

Making use of the equation (1.6) and neglectiong the higher order term in A,

$$\langle \hat{\mathbf{P}}(\mathbf{r}) \rangle(t) = \langle \hat{\mathbf{P}}(\mathbf{r}) \rangle_0 + \frac{i}{\hbar} \int_{-\infty}^{\infty} dt' \int_{\mathbb{R}^3} d\mathbf{r}' \langle \left[ \hat{\mathbf{P}}(\mathbf{r}, t), \hat{\mathbf{j}}(\mathbf{r}', t') \cdot \hat{\mathbf{A}}(\mathbf{r}', t') \right] \rangle_0 \, \vartheta(t - t'), \quad (1.15)$$

where  $\vartheta(t)$  denotes the *Heaviside step function*. Note, that the angle brackets  $\langle ... \rangle_0 = \operatorname{Tr}(\hat{\rho}_0...) = \sum_{n,m} \langle n,m | \hat{\rho}_0... | n,m \rangle$  represent the mean value in the thermodynamic equilibrium without interaction. The states indeed describe matter as well as the electromagnetic field,  $|n,m\rangle = |n\rangle_{\mathrm{M}} \otimes |m\rangle_{\mathrm{F}}$ , as a combination of non-interacting states. And since  $\hat{\mathcal{H}}_{\mathrm{M},0}$  and  $\hat{\mathcal{H}}_{\mathrm{F},0}$  act trivially on  $\mathscr{H}_{\mathrm{F}}$  and  $\mathscr{H}_{\mathrm{M}}$  respectively, we are able to split the two systems

$$\langle \hat{P}^{\alpha}(\mathbf{r}) \rangle(t) = \langle \hat{P}^{\alpha}(\mathbf{r}) \rangle_{0} + \frac{i}{\hbar} \int_{-\infty}^{\infty} dt' \int_{\mathbb{R}^{3}} d\mathbf{r}' \left\langle \left[ \hat{P}^{\alpha}(\mathbf{r}, t), \hat{j}^{\beta}(\mathbf{r}', t') \right] \right\rangle_{\mathbf{M}, 0} \vartheta(t - t') \left\langle \hat{A}_{\beta}(\mathbf{r}', t') \right\rangle_{\mathbf{F}, 0}. \quad (1.16)$$

We have introduced greek letters to mark 3-vector components. Summation over indices is implicitly understood if upper and lower index is repeated<sup>4</sup>. The average of the electromagnetic field operator is apparently the vector porential  $\langle \hat{A}(r,t) \rangle_{F,0} = A(r,t)$ . Because of the homogeneity of time and the cyclic property of the trace one can easily show that the average of the commutator depends only on the time difference t-t' as  $\langle [\hat{P}(r,t-t'),\hat{j}(r',0)] \rangle_{M,0}$ . We introduce a tensor

$$\Pi^{\alpha\beta}(\mathbf{r},\mathbf{r}',t-t') = \frac{i}{\hbar} \left\langle \left[ \hat{P}^{\alpha}(\mathbf{r},t-t'), \hat{j}^{\beta}(\mathbf{r}',0) \right] \right\rangle_{\mathbf{M},0} \vartheta(t-t'), \tag{1.17}$$

<sup>3.</sup> All linear response correlation functions are intrinsic properties of the non-interacting system [8].

<sup>4.</sup> Note that throughout this work we do not distinguish between upper and lower indices. Their position is only for convenience.

make a temporal *Fourier transform* of (1.16), and realize that according to (1.1a) and the Coulomb gauge  $E(r, \omega) = i\omega A(r, \omega)$ , so

$$\langle \hat{P}^{\alpha}(\mathbf{r}) \rangle(\omega) = \langle \hat{P}^{\alpha}(\mathbf{r}) \rangle_{0} \delta(\omega) + \int_{\mathbb{R}^{3}} d\mathbf{r}' \varepsilon_{0} \chi^{\alpha\beta}(\mathbf{r}, \mathbf{r}', \omega) E_{\beta}(\mathbf{r}', \omega), \tag{1.18}$$

with

$$\varepsilon_0 \chi^{\alpha\beta}(\mathbf{r}, \mathbf{r}', \omega) = \frac{\Pi^{\alpha\beta}(\mathbf{r}, \mathbf{r}', \omega)}{i(\hbar\omega + i0^+)},\tag{1.19}$$

which is the *Kubo formula* for electric susceptibility. The symbol  $\varepsilon_0$  denotes the *permittivity of vaccuum*. We have added a small positive imaginary frequency  $i0^+$  in order to ensure causality of the response [8].

# 1.4 Connection to optical conductivity

Optical conductivity  $\sigma$  is defined as the relation between local electric field and the electric current density

$$j^{\alpha}(\mathbf{r},\omega) = \int_{\mathbb{R}^3} d\mathbf{r}' \sigma^{\alpha\beta}(\mathbf{r},\mathbf{r}',\omega) E_{\beta}(\mathbf{r}',\omega). \tag{1.20}$$

By following similar steps to the above, it can be shown that the optical conductivity is [8]

$$\sigma^{\alpha\beta}(\mathbf{r},\mathbf{r}',\omega) = \frac{i}{\omega} \left[ \tilde{\Pi}^{\alpha\beta}(\mathbf{r},\mathbf{r}',\omega) + \frac{n_0 e^2}{m} \delta^{\alpha\beta} \delta(\mathbf{r} - \mathbf{r}') \right], \tag{1.21}$$

where  $\tilde{\Pi}^{\alpha\beta}$  written in the time domain,

$$\tilde{\Pi}^{\alpha\beta}(\mathbf{r},\mathbf{r}',t) = -\frac{i}{\hbar} \left\langle \left[ \hat{j}^{\alpha}(\mathbf{r},t), \hat{j}^{\beta}(\mathbf{r}',0) \right] \right\rangle_{\mathbf{M},0} \vartheta(t), \tag{1.22}$$

is the *current-current correlation function*.

At finite temperatures and in thermodynamic equilibrium, it may be of interest to define the *thermal representation* as a transformation into imaginary time  $t \to \tau = it$  [8, 9]

$$\tilde{\Pi}^{\alpha\beta}(\mathbf{r},\mathbf{r}',\tau) = -\frac{1}{\hbar} \left\langle T \left\{ \hat{j}^{\alpha}(\mathbf{r},\tau) \hat{j}^{\beta}(\mathbf{r}',0) \right\} \right\rangle_{M,0}.$$
(1.23)

where T  $\{...\}$  is the *time ordering operator*<sup>5</sup>. The time evolution of a thermal operator is

$$\hat{\mathcal{O}}(\tau) = \hat{\mathcal{O}}(it) = e^{\frac{\tau}{\hbar}\hat{\mathcal{H}}}\hat{\mathcal{O}}e^{-\frac{\tau}{\hbar}\hat{\mathcal{H}}}.$$
(1.24)

<sup>5.</sup>  $T\left\{\hat{\mathcal{O}}_1(\tau)\hat{\mathcal{O}}_2(0)\right\} = \hat{\mathcal{O}}_1(\tau)\hat{\mathcal{O}}_2(0)\vartheta(-i\tau)\pm\hat{\mathcal{O}}_2(0)\hat{\mathcal{O}}_1(\tau)\vartheta(i\tau)$  where "+" is for boson-like operators and "-" for fermionic operators [9].

From classical mechanics, we know that electric charges moving inside a medium induce electric current. The mean electric current density is then induced by the flow of charge density. This might be due to two processes: electric polarization changing in time and/or inhomogeneous magnetization. Mathematically

$$j = \nabla \times M + \frac{\partial}{\partial t} P. \tag{1.25}$$

For an infinite non-magnetic medium the separation to the magnetic and electric part is, in general, ambiguous [6, 11]. In this case, the common choice is to set magnetization to zero M=0 and declare that all changes of the charge density are due to changes in polarization,  $i. e. j = \partial_t P$ . This relation can be derived for operators too and in thermal representation we get [8]

$$\hat{j}(\tau) = i \frac{\partial}{\partial \tau} \hat{P}(\tau). \tag{1.26}$$

Let us take (1.26) and insert it into (1.23)

$$\tilde{\Pi}^{\alpha\beta}(\mathbf{r},\mathbf{r}',\tau) = -\frac{i}{\hbar} \left\langle T \left\{ \frac{\partial}{\partial \tau} \hat{P}^{\alpha}(\mathbf{r},\tau) \hat{j}^{\beta}(\mathbf{r}',0) \right\} \right\rangle_{M.0}.$$
(1.27)

The average and the partial derivative can be interchanged since the averaging is through states in thermodynamic equilibrium. Next, we will convert this expression into *Matsubara representation* [8, 9]

$$\tilde{\Pi}^{\alpha\beta}(\mathbf{r},\mathbf{r}',i\nu_n) = \int_0^{\hbar\beta} d\tau \, \tilde{\Pi}^{\alpha\beta}(\mathbf{r},\mathbf{r}',\tau) e^{i\nu_n \frac{\tau}{\hbar}}, \qquad (1.28)$$

where  $v_n = 2\pi n/\beta$  with  $n \in \mathbb{Z}$  is the *bosonic Matsubara frequency*. We apply this on (1.27) and use integration by parts

$$i\hbar\tilde{\Pi}^{\alpha\beta}(\mathbf{r},\mathbf{r}',i\nu_{n}) = \int_{0}^{\hbar\beta} d\tau \left\langle T \left\{ \frac{\partial}{\partial \tau} \hat{P}^{\alpha}(\mathbf{r},\tau) \hat{j}^{\beta}(\mathbf{r}',0) \right\} \right\rangle_{\mathbf{M},0} e^{i\nu_{n}\frac{\tau}{\hbar}}$$

$$= \left[ \left\langle T \left\{ \hat{P}^{\alpha}(\mathbf{r},\tau) \hat{j}^{\beta}(\mathbf{r}',0) \right\} \right\rangle_{\mathbf{M},0} e^{i\nu_{n}\frac{\tau}{\hbar}} \right]_{0}^{\hbar\beta} - i\nu_{n}\Pi^{\alpha\beta}(\mathbf{r},\mathbf{r}',i\nu_{n}),$$
(1.29)

where we have recognized the polarization-current correlation function from (1.17)

$$\Pi^{\alpha\beta}(\mathbf{r},\mathbf{r}',i\nu_n) = \int_0^{\hbar\beta} d\tau \,\frac{1}{\hbar} \left\langle T \left\{ \hat{P}^{\alpha}(\mathbf{r},\tau) \hat{j}^{\beta}(\mathbf{r}',0) \right\} \right\rangle_{M,0} e^{i\nu_n \frac{\tau}{\hbar}}, \tag{1.30}$$

which is directly related to the electric susceptibility  $\chi^{\alpha\beta}$ . We can further simplify relation (1.29) by realizing that  $e^{i\nu_n\beta}=e^0=1$  and that

$$\left[ \left\langle \mathbf{T} \left\{ \hat{P}^{\alpha}(\mathbf{r}, \tau) \hat{j}^{\beta}(\mathbf{r}', 0) \right\} \right\rangle_{\mathbf{M}, 0} \right]_{0}^{\hbar \beta} \\
= \left\langle \mathbf{T} \left\{ \hat{P}^{\alpha}(\mathbf{r}, \hbar \beta) \hat{j}^{\beta}(\mathbf{r}', 0) - \hat{P}^{\alpha}(\mathbf{r}, 0) \hat{j}^{\beta}(\mathbf{r}', 0) \right\} \right\rangle_{\mathbf{M}, 0} \\
= \left\langle \mathbf{T} \left\{ \hat{P}^{\alpha}(\mathbf{r}, 0^{+}) \hat{j}^{\beta}(\mathbf{r}', 0) - \hat{j}^{\beta}(\mathbf{r}', 0^{+}) \hat{P}^{\alpha}(\mathbf{r}, 0) \right\} \right\rangle_{\mathbf{M}, 0} \\
= \left\langle \left[ \hat{P}^{\alpha}(\mathbf{r}), \hat{j}^{\beta}(\mathbf{r}') \right] \right\rangle_{\mathbf{M}, 0}, \tag{1.31}$$

where  $f(0^+)$  is understood as the limit  $\lim_{\epsilon \to 0^+} f(\epsilon)$  for some function f. In the last step, we used the cyclic property of the trace. Inserting this back into (1.29), we find that

$$\Pi^{\alpha\beta}(\mathbf{r},\mathbf{r}',i\nu_n) = -\frac{i\hbar}{i\nu_n}\tilde{\Pi}^{\alpha\beta}(\mathbf{r},\mathbf{r}',i\nu_n) + \frac{1}{i\nu_n}\left\langle \left[\hat{P}^{\alpha}(\mathbf{r}),\hat{j}^{\beta}(\mathbf{r}')\right]\right\rangle_{\mathbf{M},0}.$$
 (1.32)

The usual frequency dependence is recovered from the Matsubara repsresentation by substituing  $iv_n \to \hbar\omega + i0^+$ . The small imaginary energy is added in order to ensure convergence and to obrain the retarded (causal) response function.

Looking back at (1.3a), the dielectric tensor  $\varepsilon^{\alpha\beta}$  is defined as a linear relation between E and D, which can be written in simplified notation as  $D_{\alpha} = \varepsilon_0 \varepsilon^{\alpha\beta} E_{\beta}$ . We have already found the electric susceptibility as the tensor ensuring a linear relation between E and P. It is then straightforward to get

$$\varepsilon^{\alpha\beta}(\mathbf{r},\mathbf{r}',\omega) = \delta(\mathbf{r}-\mathbf{r}')\delta^{\alpha\beta} + \chi^{\alpha\beta}(\mathbf{r},\mathbf{r}',\omega). \tag{1.33}$$

Using equation (1.19) and the recently-derived relation between the correlation functions (1.32),

$$\varepsilon^{\alpha\beta}(\mathbf{r},\mathbf{r}',\omega) = \delta(\mathbf{r}-\mathbf{r}')\delta^{\alpha\beta} + \frac{\Pi^{\alpha\beta}(\mathbf{r},\mathbf{r}',\omega)}{i(\hbar\omega+i0^{+})} \\
= \delta(\mathbf{r}-\mathbf{r}')\delta^{\alpha\beta} + \frac{-i\hbar}{i(\hbar\omega+i0^{+})^{2}} \left[ \tilde{\Pi}^{\alpha\beta}(\mathbf{r},\mathbf{r}',\omega) + \frac{i}{\hbar} \left\langle \left[ \hat{P}^{\alpha}(\mathbf{r}), \hat{j}^{\beta}(\mathbf{r}') \right] \right\rangle_{\mathrm{M},0} \right]. \tag{1.34}$$

Compared to (1.21), we see that [8]

$$\varepsilon^{\alpha\beta}(\mathbf{r},\mathbf{r}',\omega) = \delta(\mathbf{r}-\mathbf{r}')\delta^{\alpha\beta} - \hbar \frac{\sigma^{\alpha\beta}(\mathbf{r},\mathbf{r}',\omega)}{i(\hbar\omega + i0^{+})},$$
(1.35)

$$\frac{i}{\hbar} \left\langle \left[ \hat{P}^{\alpha}(\mathbf{r}), \hat{j}^{\beta}(\mathbf{r}') \right] \right\rangle_{\mathbf{M},0} = \frac{n_0 e^2}{m} \delta^{\alpha\beta} \delta(\mathbf{r} - \mathbf{r}'). \tag{1.36}$$

# 1.5 Long wavelength limit

Let us consider the characteristic distances in standard optical measurements.

We will refer to an infinite medium with spatially periodic structure as a crystal. It is invariant under some set of translations which depend on its symmetry group. Usually, the spatial period is of the order of interatomic distances<sup>6</sup>  $a \sim 5$  Å.

When carrying out optical measuremets in practice, the wavelength  $\lambda$  of light used ranges from approximately 100 nm up to about 1 mm [ref..]. The spatial period of the crystal is much smaller than the wavelength of the probing light,  $|q|a \sim a/\lambda \ll 1$ . Hence, the translation symmetry may be considered as continuous and the crystal as homogeneous.

Recall that the susceptibility  $\chi^{\alpha\beta}({\bf r},{\bf r}',t)$  is an intrinsic property of the unperturbed system in thermodynamic equilibrium. If we assume the crystal to be homogeneous, the susceptibility depends only on the difference  $({\bf r}-{\bf r}')$ . Moreover, we will consider that there is no macroscopic<sup>7</sup> polarization inside the system in equilibrium  $\langle \hat{\bf P}({\bf r}) \rangle_0 = 0$ . This way we can take a spatial Fourier transform of (1.18)

$$P^{\alpha}(\boldsymbol{q},\omega) = \chi^{\alpha\beta}(\boldsymbol{q},\omega)E_{\beta}(\boldsymbol{q},\omega), \qquad (1.37)$$

where

$$\chi^{\alpha\beta}(\mathbf{q},\omega) = \frac{\Pi^{\alpha\beta}(\mathbf{q},\omega)}{i(\hbar\omega + i0^{+})}$$
(1.38)

and the correlation function written in the time domain

$$\Pi^{\alpha\beta}(\boldsymbol{q},t) = \frac{1}{\Omega} \int_{\mathbb{R}^3} d(\boldsymbol{r} - \boldsymbol{r}') e^{i\boldsymbol{q}\cdot(\boldsymbol{r} - \boldsymbol{r}')} \Pi^{\alpha\beta}(\boldsymbol{r} - \boldsymbol{r}',t)$$
(1.39)

The symbol  $\Omega$  denotes the volume of the crystal. The dielectric tensor (1.34) is then

$$\varepsilon^{\alpha\beta}(\boldsymbol{q},\omega) = \delta^{\alpha\beta} + \frac{\Pi^{\alpha\beta}(\boldsymbol{q},\omega)}{i(\hbar\omega + i0^{+})},$$
(1.40)

and using the results from the previous section 1.4,

$$\varepsilon^{\alpha\beta}(\boldsymbol{q},\omega) = \text{const.} \cdot \delta^{\alpha\beta} + \frac{-\hbar\tilde{\Pi}^{\alpha\beta}(\boldsymbol{q},\omega)}{(\hbar\omega + i0^{+})^{2}}$$
(1.41)

It can be shown [8] that for the macroscopic response in the time domain

$$\tilde{\Pi}^{\alpha\beta}(\boldsymbol{q},t) = -\Omega \frac{i}{\hbar} \left\langle \left[ \hat{j}^{\alpha}(-\boldsymbol{q},t), \hat{j}^{\beta}(\boldsymbol{q},0) \right] \right\rangle_{\mathbf{M},0} \vartheta(t). \tag{1.42}$$

Since the current-density operator  $\hat{j}$  is Hermitian, it holds that  $\hat{j}(-q) = \hat{j}^{\dagger}(q)$ .

<sup>6.</sup> In contrast to metamaterials where characteristic distances can get much greater. This issue is, however, beyond the scope of this work.

<sup>7.</sup> On scales comparable to the wavelength  $\lambda$ .

# 1.6 Spatial dispersion

As mentioned in the previous section 1.5, the energy dispersion of light  $\omega = 2\pi c/\lambda$  with wavelength in the optical range does not reach zero frequency. Consequently, we will not be interested in the static dielectric response  $\varepsilon^{\alpha\beta}(q,0)$ . This enables us to write for the imaginary part of the dielectric tensor

$$\mathfrak{Im}\,\varepsilon^{\alpha\beta}(\boldsymbol{q},\omega>0) = \frac{1}{\omega^2}\mathfrak{Im}\left[-\hbar\tilde{\Pi}^{\alpha\beta}(\boldsymbol{q},\omega)\right]. \tag{1.43}$$

In addition, the pole at  $\omega=0$  corresponds to free charge carriers. In our case of a semiconductor there are no free carriers in the equilibrium state without external fields.

Let us take a closer look at the current-current correlation function. For a better understanding, it may be useful to express the function in the *Lehmann spectral representation*. We will denote the orthonormal eigenfunctions of  $\hat{\mathcal{H}}_{M,0}$ , that span the entire Hilbert space  $\mathscr{H}_M$ , as  $|\psi_n\rangle$  and their corresponding eigenvalues as  $E_n$ . Without loss of generality we will also skip the subscript "M" as all operators and states are strictly matter-related.

Both the current-density operator (1.7), and the non-interacting Hamiltonian  $\hat{\mathcal{H}}_0$  conserve the number of particles. It is therefore sufficient to use the *canonical ditribution*  $\hat{\rho}_0 = \exp(-\beta \hat{\mathcal{H}}_0)/z$ , and the *canonical partition fuction*  $z = \text{Tr}(\hat{\rho}_0)$  instead of the grand canonical counterparts defined by (1.9).

Making once more use of the thermal notation

$$-\hbar\tilde{\Pi}^{\alpha\beta}(\boldsymbol{q},\tau) = \frac{1}{\Omega} \left\langle T \left\{ \hat{j}^{\alpha}(-\boldsymbol{q},\tau) \hat{j}^{\beta}(\boldsymbol{q},0) \right\} \right\rangle_{0}$$

$$= \frac{1}{\Omega z} \sum_{n} \left\langle \psi_{n} | e^{-\beta\hat{\mathcal{H}}_{0}} T \left\{ \hat{j}^{\alpha}(-\boldsymbol{q},\tau) \hat{j}^{\beta}(\boldsymbol{q},0) \right\} |\psi_{n}\rangle, \qquad (1.44)$$

where the  $\tau$ -dependence of the current-density operator is given by (1.24). Since  $|\psi_n\rangle$  is the eigenbasis of  $\hat{\mathcal{H}}_0$ , the sum is

$$\sum_{n} e^{-\beta E_{n}} \langle \psi_{n} | \left[ e^{\frac{\tau}{\hbar} \hat{\mathcal{H}}_{0}} \hat{j}^{\alpha}(-\boldsymbol{q}) e^{-\frac{\tau}{\hbar} \hat{\mathcal{H}}_{0}} \hat{j}^{\beta}(\boldsymbol{q}) \vartheta(-i\tau) + \hat{j}^{\beta}(\boldsymbol{q}) e^{\frac{\tau}{\hbar} \hat{\mathcal{H}}_{0}} \hat{j}^{\alpha}(-\boldsymbol{q}) e^{-\frac{\tau}{\hbar} \hat{\mathcal{H}}_{0}} \vartheta(i\tau) \right] |\psi_{n}\rangle. \quad (1.45)$$

Using the completeness of the eigenbasis

$$\sum_{m,n} e^{-\beta E_{n}} e^{\frac{\tau}{\hbar}(E_{n}-E_{m})} \langle \psi_{n} | \hat{j}^{\alpha}(-\boldsymbol{q}) | \psi_{m} \rangle \langle \psi_{m} | \hat{j}^{\beta}(\boldsymbol{q}) | \psi_{n} \rangle \vartheta(-i\tau) + \\
+ \sum_{m,n} e^{-\beta E_{n}} e^{\frac{\tau}{\hbar}(E_{m}-E_{n})} \langle \psi_{n} | \hat{j}^{\beta}(\boldsymbol{q}) | \psi_{m} \rangle \langle \psi_{m} | \hat{j}^{\alpha}(-\boldsymbol{q}) | \psi_{n} \rangle \vartheta(i\tau), \quad (1.46)$$

or better

$$\sum_{m,n} e^{\frac{\tau}{\hbar}(E_n - E_m)} \langle \psi_n | \hat{j}^{\alpha}(-\boldsymbol{q}) | \psi_m \rangle \langle \psi_m | \hat{j}^{\beta}(\boldsymbol{q}) | \psi_n \rangle \left[ e^{-\beta E_n} \vartheta(-i\tau) + e^{-\beta E_m} \vartheta(i\tau) \right]. \quad (1.47)$$

Notice that we have to evaluate the following integral when transforming to Matsubara representation (1.28)

$$\int_{0}^{\hbar\beta} d\tau \, e^{i\nu_{\ell}\frac{\tau}{\hbar}} e^{\frac{\tau}{\hbar}(E_{n}-E_{m})} \left[ e^{-\beta E_{n}} \vartheta(-i\tau) + e^{-\beta E_{m}} \vartheta(i\tau) \right]. \tag{1.48}$$

The second term in the square bracket is identically zero on the integration interval. Provided that that  $\nu_\ell = 2\pi\ell/\beta$  is the bosonic Matsubara frequency, the integral gives

$$e^{-\beta E_n} \int_0^{\hbar \beta} d\tau \, e^{i\nu_{\ell} \frac{\tau}{\hbar}} e^{\frac{\tau}{\hbar} (E_n - E_m)} = \hbar \frac{e^{-\beta E_m} - e^{-\beta E_n}}{E_m - E_n + i\nu_{\ell}}.$$
 (1.49)

Putting everything together, the tensor  $\tilde{\Pi}^{\alpha\beta}$  in Matsubara representation reads

$$-\hbar\tilde{\Pi}^{\alpha\beta}(\boldsymbol{q},i\nu_{\ell}) = \frac{\hbar}{\Omega z} \sum_{m,n} \langle \psi_n | \hat{j}^{\alpha}(-\boldsymbol{q}) | \psi_m \rangle \langle \psi_m | \hat{j}^{\beta}(\boldsymbol{q}) | \psi_n \rangle \frac{e^{-\beta E_m} - e^{-\beta E_n}}{E_m - E_n + i\nu_{\ell}}.$$
 (1.50)

We are going to express the tensor in the eigencoordinates of the crystal. This means that all the off-diagonal elements are zero<sup>8</sup> The transformation back to real frequency domain is, as usual, done by analytical continuation  $i\nu_\ell \to \hbar\omega + i0^+$ ,

$$-\hbar\tilde{\Pi}^{\alpha\alpha}(\boldsymbol{q},\omega) = \frac{\hbar}{\Omega z} \sum_{m,n} \left| \langle \psi_m | \hat{j}^{\alpha}(\boldsymbol{q}) | \psi_n \rangle \right|^2 \frac{e^{-\beta E_m} - e^{-\beta E_n}}{E_m - E_n + \hbar\omega + i0^+}, \tag{1.51}$$

where the index  $\alpha$  is fixed. The imaginary part can be obtained by Sochocki–Plemelj theorem<sup>9</sup> which yields the dielectric tensor in (1.43) as

$$\mathfrak{Im}\,\varepsilon^{\alpha\alpha}(\boldsymbol{q},\omega) = -\frac{\pi}{\omega^{2}}\frac{\hbar}{\Omega}\left[\frac{1}{1+n_{B}(\hbar\omega)}\right] \times \\ \times \sum_{m,n} \left|\left\langle\psi_{n}\right|\left(\hat{j}^{\alpha}\right)^{\dagger}(\boldsymbol{q})\left|\psi_{m}\right\rangle\right|^{2} \frac{e^{-\beta E_{m}}}{z}\,\delta(\hbar\omega - E_{n} + E_{m})\,, \quad (1.52)$$

$$\frac{1}{x+i0^+} = \mathcal{P}\left(\frac{1}{x}\right) - i\pi\delta(x),$$

where  $\mathcal{P}$  denotes the *Cauchy principal value*. Of course this is understood to be under the integral sign.

<sup>8.</sup> The dielectric tensor in a non-absorbing medium is Hermitian [6], in which case there is always a basis in which it is diagonal. Generally, however, the real and imaginary parts must not be simultaneously diagonalizable.

<sup>9.</sup> The theorem states that

where  $n_{\rm B}(\hbar\omega)=(e^{\beta\hbar\omega}-1)^{-1}$  is the *Bose-Einstein distribution*. The imaginary part of the dielectric function describes absorption processes. Inside the sum, the term  $\delta(\hbar\omega-(E_n-E_m))$  ensures that only prosesses that conserve energy are allowed. The factor  $e^{-\beta E_m}/z$  tells us about the occupation of the initial state  $|\psi_m\rangle$ . Finally, the matrix element  $\left|\langle\psi_n|\left(\hat{j}^\alpha\right)^\dagger(q)|\psi_m\rangle\right|^2$  gives the probability of the transition  $\psi_m\to\psi_n$ . This transition might be forbidden due to symmetries of the initial and final states.

The matrix elements of  $(\hat{j}^{\alpha})^{\dagger}$  are contingent of the eigenbasis  $\{|\psi_n\rangle\}$ . In other words, the result depends on the chosen model. There had been made calculations for  $e.\ g.$  the Oscillator model [2] or the Penn model [12]. Even without a specific model, some conclusions can be drawn. Let us take a generic matrix element  $\langle \psi_n | (\hat{j}^{\alpha})^{\dagger} (q) | \psi_m \rangle$  and insert the current density operator (1.7) in q-representation,

$$-\sum_{\ell} \frac{q_{\ell}}{2m_{\ell}} \langle \psi_{n} | \left( e^{-i\boldsymbol{q}\cdot\hat{\boldsymbol{r}}_{\ell}} \hat{p}_{\ell}^{\alpha} + \hat{p}_{\ell}^{\alpha} e^{-i\boldsymbol{q}\cdot\hat{\boldsymbol{r}}_{\ell}} \right) | \psi_{m} \rangle. \tag{1.53}$$

Do not confuse the charge of  $\ell$ -th partice  $q_{\ell}$  with the wavevector q. The vector coordinates are labeled with a greek superscript. A common practice is to take the limit  $|q| \to 0$ , which is meaningful for optical frequencies. We will rather keep also the first terms of the Taylor series of the exponential,

$$-\sum_{\ell} \frac{q_{\ell}}{2m_{\ell}} \langle \psi_{n} | \left[ \left( \hat{1} - i\boldsymbol{q} \cdot \hat{\boldsymbol{r}}_{\ell} - \frac{1}{2} (\boldsymbol{q} \cdot \hat{\boldsymbol{r}}_{\ell})^{2} + ... \right) \hat{p}_{\ell}^{\alpha} + \right.$$

$$+ \left. \hat{p}_{\ell}^{\alpha} \left( \hat{1} - i\boldsymbol{q} \cdot \hat{\boldsymbol{r}}_{\ell} - \frac{1}{2} (\boldsymbol{q} \cdot \hat{\boldsymbol{r}}_{\ell})^{2} + ... \right) \right] |\psi_{m}\rangle . \quad (1.54)$$

This can be separated into terms that depend on different powers of elements of the wavevector q. The first few are

1. independent of q, which is connected with the dipole transition<sup>10</sup>

$$-\sum_{\ell} \frac{q_{\ell}}{m_{\ell}} \langle \psi_{n} | \hat{p}_{\ell}^{\alpha} | \psi_{m} \rangle, \qquad (1.55a)$$

2. linearly dependent on q, which is connected with the quadrupole transition [2]

$$i\sum_{\ell} \frac{q_{\ell}}{2m_{\ell}} \langle \psi_{n} | \left( \hat{r}_{\ell}^{\beta} \hat{p}_{\ell}^{\alpha} + \hat{p}_{\ell}^{\alpha} \hat{r}_{\ell}^{\beta} \right) | \psi_{m} \rangle q_{\beta}, \tag{1.55b}$$

3. quadratically dependent on q which is connected with the octupole transition [ref..]

$$\sum_{\ell} \frac{q_{\ell}}{4m_{\ell}} \langle \psi_{n} | \left( \hat{r}_{\ell}^{\beta} \hat{r}_{\ell}^{\gamma} \hat{p}_{\ell}^{\alpha} + \hat{p}_{\ell}^{\alpha} \hat{r}_{\ell}^{\beta} \hat{r}_{\ell}^{\gamma} \right) | \psi_{m} \rangle q_{\beta} q_{\gamma}. \tag{1.55c}$$

Thus, the matrix element of the current-density operator  $(\hat{j}^{\alpha})^{\dagger}$  as a function of the external field wavevector can be can be expressed as a series

$$\langle \psi_n | \left( \hat{j}^{\alpha} \right)^{\dagger} (\boldsymbol{q}) | \psi_m \rangle = \left( T^{(0)} \right)^{\alpha} + \left( T^{(1)} \right)^{\alpha \beta} q_{\beta} + \left( T^{(2)} \right)^{\alpha \beta \gamma} q_{\beta} q_{\gamma} + ..., \tag{1.56}$$

where  $T^{(n)}$  is a tensor of order (n+1).

By analogy, the whole transition probability  $\left| \langle \psi_n | \left( \hat{j}^\alpha \right)^\dagger (q) | \psi_m \rangle \right|^2$ , as well as the imaginary part of the dielectric tensor (1.52), can be decomposed into a series with respect to the wavevector q

$$\mathfrak{Im}\,\varepsilon^{\alpha\beta}(\boldsymbol{q},\omega) = \mathfrak{Im}\Big(\varepsilon^{(0)}(\omega)\Big)^{\alpha\beta} + \mathfrak{Im}\Big(\varepsilon^{(1)}(\omega)\Big)^{\alpha\beta\gamma}\,q_{\gamma} + \mathfrak{Im}\Big(\varepsilon^{(2)}(\omega)\Big)^{\alpha\beta\gamma\delta}\,q_{\gamma}q_{\delta} + ..., \tag{1.57}$$

where  $\varepsilon^{(n)}$  is a tensor of order (n+2). The real part of the dielectric tensor is obtained by employing *Kramers-Kronig relations* 

$$\mathfrak{Re}\,\varepsilon^{\alpha\beta}(\boldsymbol{q},\omega) = \delta^{\alpha\beta} + \frac{1}{\pi}\mathcal{P}\int_{-\infty}^{\infty} d\omega' \,\frac{\mathfrak{Im}\,\varepsilon^{\alpha\beta}(\boldsymbol{q},\omega')}{\omega' - \omega}.\tag{1.58}$$

The symbol  $\mathcal{P}$  indicates that the integral is evaluated in the sense of the *Cauchy principal value*. We immediately see, that if the imaginary part of the dielectric tensor  $\mathfrak{Im}\ \epsilon^{\alpha\beta}$  is diagnal in some basis, then the real part  $\mathfrak{Re}\ \epsilon^{\alpha\beta}$  is also diagonal in the same basis. Moreover, the wavevector dependence is preserved since it is treated as an separate variable independent of the frequency  $\omega$ .

In the following, we will use the notation

$$\varepsilon^{\alpha\beta}(\mathbf{q},\omega) = \varepsilon^{\alpha\beta}(\omega) + ig^{\alpha\beta\gamma}(\omega)q_{\gamma} + a^{\alpha\beta\gamma\delta}(\omega)q_{\gamma}q_{\delta}. \tag{1.59}$$

Evidently, the  $0^{\text{th}}$  order term in the wavevector expansion corresponds to the long-wavelength limit  $|q| \to 0$  in which  $\varepsilon^{\alpha\beta}(q,\omega) = \varepsilon^{\alpha\beta}(\omega)$  is the classical dielectric tensor given solely by the dipole transitions inside the crystal (1.55a). The next term linear in components of q corresponds to quadrupole transitions (1.55b), and  $g^{\alpha\beta\gamma}$  is often called the *gyration tensor* [13, 14]. In the quadratic term, the  $a^{\alpha\beta\gamma\delta}$  contains quadrupole (1.55b), as well as octupole transitions (1.55c). It is commonly referred to as the *spatial dispersion tensor* (SD tensor) [15], in spite of the fact that spatial dispersion is the complete q-vector dependence. More generally, it is the non-local response of the crystal to external electromagnetic field. Nevertheless, for the sake of consistency, we will stick to this nomenclature.

<sup>10.</sup> For Heisenberg operators and a Hamiltonian of the form  $\hat{\mathcal{H}}_0 = \sum_n \frac{\hat{p}_n^2}{2m_n} + \hat{V}(\hat{r}_0, \hat{r}_1, ..., \hat{r}_n)$ , the equation of motion of the position operator  $\hat{r}_n^{\alpha}$  provides  $\frac{1}{i\hbar} \left[ \hat{r}_n^{\alpha}, \hat{\mathcal{H}}_0 \right] = \frac{1}{m_n} \hat{p}_n^{\alpha}$ . For eigenstates  $|\psi_n\rangle$  of the Hamiltonian  $\hat{\mathcal{H}}_0$ , it is easily seen that  $\langle \psi_m | \hat{p}_\ell^{\alpha} | \psi_n \rangle \propto \langle \psi_m | \hat{r}_\ell^{\alpha} | \psi_n \rangle$  which is related to the dipole matrix element.

To conclude the chapter, the takeaway message is that the non-local response (spatial dispersion) corresponds to quadrupole and higher order transitions (1.55) inside the material caused by external electromagnetic field [2]. This can be translated into power series of the dieletric tensor in componets of the wavevector (1.59). From now on we will not worry much about the internal structure of the transitions, but simply about the wavevector dependence.

#### 2 Model

In the previous chapter, we showed how the q-vector dependency emerges from the non-local behavior of the response function. Here we will make a deeper analysis of cubic crystals and the particular form the dielectric tensor takes due to crystal symmetries of the cubic lattice (the geometry of the system). A modification of this concept to more complex crystalographic groups is simple and straightforward.

The following section will be devoted to simple, and rather empirical, dispersion models that we compared against our experimental data.

Afterwards, we will move into more practical parts and briefly discuss the issues related to real crystals. In particular, a method of accounting for finite dimensions of real crystals will be described.

The last section will focus on the implementation of the model with the use of a computation technique called *Berreman formalism*. We will point out the modifications that need to be made due to q-vector dependence of the response, which is not considered in the original formulation.

# 2.1 Symmetries of the dielectric tensor

From the physics standpoint, the response of the crystal must follow some rules. This restricts the dielectric tensor to a specific form. The first requirement is the preservation of reciprocity [6, 11], which states, that

$$\varepsilon(q,\omega) = \varepsilon^{\mathrm{T}}(-q,\omega). \tag{2.1a}$$

Secondly, we will assume a lossless medium, or, more precisely, we will use a frequency range where the medium does not absorb light. This means that the dielectric tensor is Hermitian [6, 13]

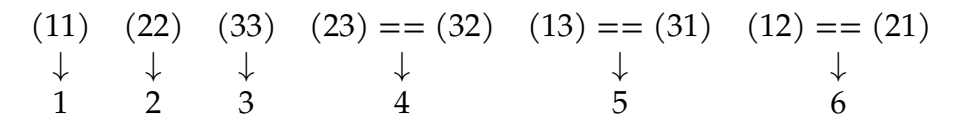
$$\varepsilon(q,\omega) = \varepsilon^{\dagger}(q,\omega). \tag{2.1b}$$

The symbols "T" and "†" stand for the transpose and the Hermitian conjugate, respectively.

Combining these two equations (2.1), it is not hard to show that the even terms in the q-expansion are real and symmetric, and the odd terms are purely imaginary and antisymmetric. This can be translated into the antisymmetry of the gyration tensor  $g^{\alpha\beta\gamma}(\omega)$  and the symmetry of the SD tensor  $a^{\alpha\beta\gamma\delta}(\omega)$  in the first two indices  $\alpha$ ,  $\beta$ . Moreover, equations (1.55) show that the SD tensor is symmetric also in the last two indices  $\gamma$ ,  $\delta$ . As a consequence, it has only six independent components. Moreover, crystals posess additional (spatial?) symmetries, so the number of independent parameters is further reduced.

<sup>1.</sup> More precisely, it can always be symmetrized.

**Table 2.1:** Assingnment of indices to rewrite the SD tensor  $a^{\alpha\beta\gamma\delta}(\omega)$  into Voigt notation [15–17]. The tuples in the first row correspond to the symmetric pairs of indices  $(\alpha\beta) == (\beta\alpha)$  and  $(\gamma\delta) == (\delta\gamma)$  respectively.



Another property that we have already used is the translation symmetry. Specifically, we declared the discrete translation symmetry to be continuous wthin the long wavelength limit. Now we are going to make use of the point group symmetries. We will assume that the equilibrium state posesses all the symmetries of the Hamiltonian. In other words, there is no spontaneous symmetry breaking of the ground state. A typical example are ferromagnetic materials, where the spin-rotational symmetry is broken.

A three-dimensional crystal lattice, *i. e.* the pattern of equilibrium positions of atoms/molecules, can be classified into seven point groups: triclinic, monoclinic, orthorombic, tetragonal, trigonal, hexagonal, and cubic. Only the latter is the subject of our interest. Taking into account the complete structure of the crystal, the cubic point grup is further divided into five crystallographic classes, the Tetrahedral classes 23 (T),  $m\bar{3}$  (T<sub>h</sub>),  $\bar{4}3m$  (T<sub>d</sub>), and the Octahedral classes 432 (O),  $m\bar{3}m$  (O<sub>h</sub>). All cubic classes are non-polar, but only three of them are achiral, namely  $m\bar{3}m$ ,  $\bar{4}3m$ , and  $m\bar{3}$ .

Returning to the equation (1.59), we now see why the second (gyrotropic) term linear in q must be identically zero for crystals belonging to one of the three achiral cubic classes. The reason is that all of them are centrosymmetric point groups and this term is clearly antisymmetric under point inversion (changes its sign if the direction of light is inverted). The gyrotropic term is of the order of  $\mathcal{O}(|q|)$ . The SD term is much smaller since it scales with  $\mathcal{O}(|q|^2)$ . We will focus on these three achiral classes because we want to study the SD tensor  $a^{\alpha\beta\gamma\delta}$  which is overwhelmed by the gyration tensor in the remaining two classes.

It turns out to be convenient to express the tensor in a matrix form using the *Voigt notation*, since  $a^{\alpha\beta\gamma\delta}$  is symmetric in te first two and in the last two indices. This is performed by the assignment captured in table 2.1. The tensor product is then calculated as a matrix multiplied by the vector  $(q_1^2 \ q_2^2 \ q_3^2 \ 2q_2q_2 \ 2q_1q_3 \ 2q_1q_2)^T$  from the right side. The symmetries of the five cubic classes result in only two distinct forms if the SD tensor, wich have the same structure as the photoelastic tensor [1, 2, 16]. In the case of the class  $m\bar{3}$  it depends on four parameters. The explicit frequency-dependence will be

sometimes ommited in this chapter to simplify the notation

$$\begin{pmatrix} a_{11} & a_{12} & a_{13} & 0 & 0 & 0 \\ a_{13} & a_{11} & a_{12} & 0 & 0 & 0 \\ a_{12} & a_{13} & a_{11} & 0 & 0 & 0 \\ 0 & 0 & 0 & a_{44} & 0 & 0 \\ 0 & 0 & 0 & 0 & 0 & a_{44} \end{pmatrix},$$

$$(2.2a)$$

but for the  $m\bar{3}m$  and  $\bar{4}3m$  cubic classes, due to the four-fold symmetry of the [001] directions,  $a_{13}=a_{12}$  and so the SD tensor corresponds to the matrix

$$\begin{pmatrix} a_{11} & a_{12} & a_{12} & 0 & 0 & 0 \\ a_{12} & a_{11} & a_{12} & 0 & 0 & 0 \\ a_{12} & a_{12} & a_{11} & 0 & 0 & 0 \\ 0 & 0 & 0 & a_{44} & 0 & 0 \\ 0 & 0 & 0 & 0 & 0 & a_{44} \end{pmatrix}.$$
 (2.2b)

We would like to point out that, although the derivation was made for a real tensor, it can be analytically continued into complex values, so that it preserves the symmetries of the real one. It might, however, happen that the real and imaginary parts cannot be diagonalized simultaneously.

## 2.2 Real crystal corrections

Up to now we have been avoiding some problems of real crystals. In this section we touch upon the topic of adjusting boundary conditions when spatial dispersion is taken into account. We do not mention issues like strain, surface rougness and absporption as they are irrelevant for our experimental results.

## 2.2.1 Boundary conditions

At the end of section 1.1 we have mentioned that in an infinite medium the border between electric and magnetic material properties is somewhat blurry. We have argued that because of this ambiguity and the insignficant magnetic response of non-magnetic materials, the material properties may be completely described by the dielectric tensor. It also allowed us to circumvent the problem of boundary conditions.

Clearly, waiving the requirement of unboundedness of ideal crystals breaks the translation symmetry. Furthermore, it causes severe complications when solving eqations at interfaces. As we will see in section 2.4.1, even with an approximate solution, one usually

has to impose some *additional boundary conditions* (ABCs) [18]. Let us note that this problem does not arise if the dielectric tensor is assumed to be local  $\varepsilon^{\alpha\beta}(r,r') \propto \delta(r-r')$ .

Nevertheless, sometimes there are ways of separating the magnetic and electric current densities. This allows then the use of the classical boundary conditions derived for the local response [19–21]. In this work, we are using the method presented by Ossikovski and Arteaga in [15]. They reformulated the dielectric and permeability tensors in a way that the electric and magnetic parts are decoupled. The correctness is argued by comparisson of eigenmodes calculated by the Fresnel equation (see  $e.\ g.\ [15,21]$ ) and by the *Berreman's method* [20] (see section 2.4).

This method uses the *Fedorov's transformation* [14, 22] which transforms the electric induction D and magnetic field H using a vector Q. In the case of spatial dispersion it is chosen to be of magnetic nature  $Q^{\alpha} = \tilde{a}_{\rm m}{}^{\alpha\beta} B_{\beta}$ , where  $\tilde{a}_{\rm m}$  is called the *magnetic SD tensor* [15]. The transformation reads

$$H'(q,\omega) = H(q,\omega) + \omega \tilde{a}_{m}(\omega)B(q,\omega), \qquad (2.3a)$$

$$D'(q,\omega) = D(q,\omega) - q \times [\tilde{a}_{m}(\omega)B(q,\omega)], \qquad (2.3b)$$

where the primed quantities are the transformed ones. The Fedorov's transformation leaves the *Ampére's law* unchanged. One may think of the transformation as a redistribution between magnetization and polarization current densities.

The electric and magnetic fields E and B are also not affected by the transformation. If the definition of the magnetic permeability  $B(q,\omega) = \mu_0 \mu(\omega) H(q,\omega)$  and the equation (2.3a) are combined, we get the new (inverse) permeability

$$\left(\boldsymbol{\mu}'\right)^{-1}(\omega) = \boldsymbol{\mu}^{-1}(\omega) + \mu_0 \,\omega \,\tilde{\boldsymbol{a}}_{\mathrm{m}}(\omega). \tag{2.4}$$

For the case of electric field, we combine the defining eqution for the dielectric tensor  $D(q,\omega) = \varepsilon_0 \varepsilon(q,\omega) E(q,\omega)$ , the equation (2.3b), and the *Faraday's law*  $q \times E(q,\omega) = \omega B(q,\omega)$  in order to get the new dielectric tensor implicitly

$$\varepsilon'(q,\omega)E(q,\omega) = \varepsilon(q,\omega)E(q,\omega) - \frac{1}{\omega\varepsilon_0} q \times \{\tilde{a}_{\rm m}(\omega) [q \times E(q,\omega)]\}.$$
 (2.5)

Noticing that the cross product can be viewed as matrix multiplication with the use of the *completely antisymmetric Levi-Civita tensor*  $^2$   $\epsilon^{\alpha\beta\gamma}$  and using the associative property of matrix multiplication, the expression for the new dielectric tensor can be writen explicitly

$$(\varepsilon')^{\alpha\beta}(\mathbf{q},\omega) = \varepsilon^{\alpha\beta}(\mathbf{q},\omega) - a_{\mathrm{m}}{}^{\alpha\beta\gamma\delta}(\omega)q_{\gamma}q_{\delta}, \tag{2.6}$$

<sup>2.</sup> For any two vectors u, v the cross product can be written as  $(u \times v)^{\alpha} = \epsilon^{\alpha\beta\gamma}u^{\beta}v^{\gamma}$ , where  $\epsilon^{012} = 1$  and the other elements are determined by antisymmetry in each two indices.

where we defined

$$a_{\rm m}{}^{\alpha\beta\gamma\delta} = \frac{1}{\omega\varepsilon_0} \, \epsilon^{\alpha\gamma\zeta} \tilde{a}_{\rm m,\zeta\eta} \epsilon^{\eta\delta\beta}. \tag{2.7}$$

Equation (2.6) can be comapred to the dielectric tensor (1.59) with all the symmetries from the previous section 2.1 taken into account

$$(\varepsilon')^{\alpha\beta}(\mathbf{q},\omega) = \varepsilon^{\alpha\beta}(\omega) + a^{\alpha\beta\gamma\delta}(\omega)q_{\gamma}q_{\delta} - a_{\mathrm{m}}{}^{\alpha\beta\gamma\delta}(\omega)q_{\gamma}q_{\delta}$$
$$= \varepsilon^{\alpha\beta}(\omega) + a_{\mathrm{e}}{}^{\alpha\beta\gamma\delta}(\omega)q_{\gamma}q_{\delta}. \tag{2.8}$$

The newly defined tensor  $a_{\rm e}{}^{\alpha\beta\gamma\delta}=a^{\alpha\beta\gamma\delta}-a_{\rm m}{}^{\alpha\beta\gamma\delta}$  is referred to as the *electric SD tensor*. Using the same symmetry arguments as before, it is easy to see that the magnetic permeability in cubic crystals must be isotropic, as the magnetic SD tensor  $\tilde{a}_{\rm m}(\omega)$  is independent of the wavevector<sup>3</sup>. As a consequence,  $\tilde{a}_{\rm m}{}^{\alpha\beta}(\omega)=\tilde{\mu}(\omega)\delta^{\alpha\beta}$ , with  $\tilde{\mu}(\omega)$  being a scalar function. On the whole, the magnetic tensor  $a_{\rm m}{}^{\alpha\beta\gamma\delta}$  defined by (2.7) can be as well transcribed using Voigt notation

$$2a_{44} \begin{pmatrix} 0 & -1 & -1 & 0 & 0 & 0 \\ -1 & 0 & -1 & 0 & 0 & 0 \\ -1 & -1 & 0 & 0 & 0 & 0 \\ 0 & 0 & 0 & \frac{1}{2} & 0 & 0 \\ 0 & 0 & 0 & 0 & \frac{1}{2} & 0 \\ 0 & 0 & 0 & 0 & 0 & \frac{1}{2} \end{pmatrix}, \tag{2.9}$$

where we have to equate  $\tilde{\mu}(\omega) = 2\varepsilon_0 \omega a_{44}(\omega)$ . The transformed inverse permeability according to (2.4) becomes

$$\left(\mu'\right)^{\alpha\beta}(\omega) = \left[1 + 2\frac{\omega^2}{c^2}a_{44}(\omega)\right]\delta^{\alpha\beta},\tag{2.10}$$

since before the Fedorov's transformation the permeability tensor is equal to the identity  $\mu^{\alpha\beta}(\omega) = \delta^{\alpha\beta}$ , and  $c = 1/\sqrt{\mu_0 \varepsilon_0}$  is the speed of light.

Returning to the electric part, if we insert the expressions (2.9) and (2.2a) (or (2.2b) respectively) into (2.8), the newly defined dielectric tensor takes a diagonal form

$$\varepsilon'(\boldsymbol{q},\omega) = \begin{pmatrix} \varepsilon(\omega) + \Delta\varepsilon_{11}(\boldsymbol{q},\omega) & 0 & 0\\ 0 & \varepsilon(\omega) + \Delta\varepsilon_{22}(\boldsymbol{q},\omega) & 0\\ 0 & 0 & \varepsilon(\omega) + \Delta\varepsilon_{33}(\boldsymbol{q},\omega) \end{pmatrix}, \quad (2.11)$$

<sup>3.</sup> Just like the permittivity is isotropic in the absence of spatial dispersion.

where the elements are dependent on the elements if the SD tensor  $a^{\alpha\beta\gamma\delta}$ . In the case of the less symetric cubic class  $m\bar{3}$ , the  $\Delta\varepsilon_{\alpha\alpha}$  elements can be written as

$$\Delta\varepsilon_{11}(\boldsymbol{q},\omega) = a_{11}|\boldsymbol{q}|^2 - (a_{11} - a_{12} - 2a_{44})q_2^2 - (a_{11} - a_{13} - 2a_{44})q_3^2,$$

$$\Delta\varepsilon_{22}(\boldsymbol{q},\omega) = a_{11}|\boldsymbol{q}|^2 - (a_{11} - a_{12} - 2a_{44})q_3^2 - (a_{11} - a_{13} - 2a_{44})q_1^2,$$

$$\Delta\varepsilon_{33}(\boldsymbol{q},\omega) = a_{11}|\boldsymbol{q}|^2 - (a_{11} - a_{12} - 2a_{44})q_1^2 - (a_{11} - a_{13} - 2a_{44})q_2^2.$$
(2.12)

In the case of classes  $m\bar{3}m$ , and  $\bar{4}3m$ , where  $a_{13}=a_{12}$ ,

$$\Delta\varepsilon_{11}(\boldsymbol{q},\omega) = (a_{11} + 2a_{44})|\boldsymbol{q}|^2 + (a_{11} - a_{12} - 2a_{44})q_1^2,$$

$$\Delta\varepsilon_{22}(\boldsymbol{q},\omega) = (a_{11} + 2a_{44})|\boldsymbol{q}|^2 + (a_{11} - a_{12} - 2a_{44})q_2^2,$$

$$\Delta\varepsilon_{33}(\boldsymbol{q},\omega) = (a_{11} + 2a_{44})|\boldsymbol{q}|^2 + (a_{11} - a_{12} - 2a_{44})q_3^2.$$
(2.13)

It is hard to overlook the frequently occurring linear combinations of SD tensor elements, so we introduce the abbreviations  $p_1 = \frac{c^2}{\omega^2}(a_{11} - a_{12} - 2a_{44})$  and  $p_2 = \frac{c^2}{\omega^2}(a_{11} - a_{13} - 2a_{44})$ .

Apparently, there is an isotropic, as well as anisotropic contribution to the dielectric tensor stemming from spatial dispersion. The isotropic part of  $(\varepsilon')^{\alpha\beta}(q,\omega)$ , depending on the point group, is

$$\left[\varepsilon(\omega) + a_{11}|\boldsymbol{q}|^2\right]\delta^{\alpha\beta}$$
, or  $\left[\varepsilon(\omega) + (a_{11} + 2a_{44})|\boldsymbol{q}|^2\right]\delta^{\alpha\beta}$ . (2.14)

The former is for symmetry class  $m\bar{3}$ , and the latter for  $m\bar{3}m$  and  $\bar{4}3m$  classes. We would like to point out that when doing highly precise and accurate measurements of the absolute refractive index under the assumption of isotropy (performing a spatial average), one is really measuring the quantity from (2.14), not the  $\varepsilon(\omega)$  directly. However, as spatial dispersion is small, we may expect the average refractive index  $n(\omega)$  to be close to  $\sqrt{\varepsilon(\omega)}$ . In fact, our experiments are not sensitive to the absolute refractive index. Hence, from now on, we will relabel the scalar functions inside the square bracket in equation (2.14), dependent on  $|q|^2$ , as  $\varepsilon(\omega) = n^2(\omega)$ . For the same reason we will regard the transformed permeability to be the same as the initial one  $(\mu')^{\alpha\beta}(\omega) = \mu^{\alpha\beta}(\omega) = \delta^{\alpha\beta}$ .

On the other hand, ellipsometry is rather sensitive to changes in refractive indices for different polarizations, *i. e.* to the anisotropic part of the dielectric tensor that in (2.12) and (2.13) are the terms proportional to the parameters  $p_1$  and  $p_2$ . Within the macroscopic approach, the size of the wavevector is proportional to the refractive index of the medium, which in our case can be writen as  $|q|^2 = n^2(\omega) \omega^2/c^2 = \varepsilon(\omega) \omega^2/c^2$ .

<sup>4.</sup> A more precise approach would be to take the wave-equation, which can be derived from the Maxwell's equations [6, 21],  $\mathbf{q} \times (\mathbf{q} \times E(\mathbf{q}, \omega)) + \frac{\omega^2}{c^2} \varepsilon(\mathbf{q}, \omega) E(\mathbf{q}, \omega) = 0$  and find the eigenpolarizations  $\pi$  and their corresponding refractive indices  $n_{\pi}$  that, in general, are different for different directions of propagation. Then, the wavevector corresponding to the eigenpolarization  $\pi$  would have a magnitude implicitly given by  $|\mathbf{q}_{\pi}|^2 = n_{\pi}^2 (\mathbf{q}_{\pi}, \omega) \, \omega^2/c^2$ .

It is also useful to separate the direction and frequency dependence by introducing the unit vector in the direction of the wave propagation,  $\hat{q}^{\alpha} = q^{\alpha}/|q|$ , which should not be confused with an operator. The resulting forms of the dielectric and permeability tensors are neatly captured in Table 2.2. In the following we shall use the transformed tensors and leave out the prime symbol.

**Table 2.2:** The transformed linear response tensor functions to be used for modeling exmerimental data. They are expressed for different cubic crystallographic classes and are valid in the absorption-free spectral region. The parameters  $p_1(\omega) = \frac{c^2}{\omega^2} \left[ a_{11}(\omega) - a_{12}(\omega) - 2a_{44}(\omega) \right]$  and  $p_2(\omega) = \frac{c^2}{\omega^2} \left[ a_{11}(\omega) - a_{13}(\omega) - 2a_{44}(\omega) \right]$  affect the strength of the anisotropy caused by spatial dspersion. The unit vector (not an operator)  $\hat{q} = q/|q|$  points in the direction of light propagation.

	$\mathbf{\varepsilon}(\mathbf{q},\omega) = \mathbf{\varepsilon}(\omega)\mathbb{1} +$	$\mu(\omega)$
m3m, 43m	$arepsilon(\omega)egin{pmatrix} p_1\hat{q}_1^2 & 0 & 0 \ 0 & p_1\hat{q}_2^2 & 0 \ 0 & 0 & p_1\hat{q}_3^2 \end{pmatrix}$	$\begin{pmatrix} 1 & 0 & 0 \\ 0 & 1 & 0 \\ 0 & 0 & 1 \end{pmatrix}$
тĪ	$\varepsilon(\omega) \begin{pmatrix} -p_1 \hat{q}_2^2 - p_2 \hat{q}_3^2 & 0 & 0\\ 0 & -p_1 \hat{q}_3^2 - p_2 \hat{q}_1^2 & 0\\ 0 & 0 & -p_1 \hat{q}_1^2 - p_2 \hat{q}_2^2 \end{pmatrix}$	$ \begin{pmatrix} 1 & 0 & 0 \\ 0 & 1 & 0 \\ 0 & 0 & 1 \end{pmatrix} $

## 2.3 Dispersion model

It is widely known that the optical response functions can be described by the *harmonic* oscillator model (Sellmeier formula) with great accuracy in the frequency range where the material is transparent [23].

We make a slight modification to this model which turns out to be analogous to the modified harmonic oscillator model used to describe optical activity in isotropic media [24, 25]. We show here only the form for the classes  $m\bar{3}m$  and  $\bar{4}3m$  as the other one is irrelevant for our experiments. A similar model can be derived for classes with lower symmtry.

Starting from the expression for the imaginary part of the dielectric tensor (1.52) rewritten in a fairly abbreviated form

$$\mathfrak{Im}\,\varepsilon^{\alpha\beta}(\boldsymbol{q},\omega) = \sum_{mn} M_{nm}^{\alpha}(-\boldsymbol{q},\omega) M_{mn}^{\beta}(\boldsymbol{q},\omega)\,\delta(\hbar\omega - E_n + E_m)\,,\tag{2.15}$$

where we assumed that the matter particles are non-interacting fermions, so  $|\psi_n\rangle$  are singe-particle wavefunctions. In the low temperature limit, the equilibrium state is the

ground state and we choose it to be the zero-energy level  $E_0 = 0$ . Then

$$\mathfrak{Im}\,\varepsilon^{\alpha\beta}(\boldsymbol{q},\omega) = \sum_{n\neq 0} M_{n0}^{\alpha}(-\boldsymbol{q},\omega) M_{0n}^{\beta}(\boldsymbol{q},\omega)\,\delta(\hbar\omega - E_n)\,. \tag{2.16}$$

Recall that in the chapter 1, we made a multipole expansion (equations (1.55)). This corresponds to expansion of  $M_{nm}^{\alpha}(q)$  in the wavevector components

$$M_{nm}^{\alpha}(\boldsymbol{q},\omega) = \left(M_{nm}^{(0)}(\omega)\right)^{\alpha} + \left(M_{nm}^{(1)}(\omega)\right)^{\alpha\beta}q_{\beta} + \left(M_{nm}^{(2)}(\omega)\right)^{\alpha\beta\gamma}q_{\beta}q_{\gamma} + \dots$$
 (2.17)

A huge simplification lies in the assumption that the matrix elements are the same for all frequencies  $M_{nm}^{\alpha}(q,\omega)=M_{nm}^{\alpha}(q)$ , q.v. [2].

Keeping only the quadratic term of the dielectric tensor in components of the wavevector leads to

$$\mathfrak{Im}\,\varepsilon^{\alpha\beta}(\boldsymbol{q},\omega) = \sum_{n\neq 0} (N_n^{\alpha\beta} + S_n^{\alpha\beta\gamma\delta} q_{\gamma} q_{\delta}) \frac{1}{E_n} \,\delta(\hbar\omega - E_n), \qquad (2.18)$$

where  $N_n/E_n$  and  $S_n/E_n$  are combinations of  $M_{n0}^{(0)}$ ,  $M_{0n}^{(0)}$ ,  $M_{n0}^{(1)}$ ,  $M_{n0}^{(1)}$ ,  $M_{n0}^{(2)}$ ,  $M_{n0}^{(2)}$ , and are connected with the strength of the n-th harmonic oscillator. By Kramers-Kronig relations (1.58),

$$\Re \epsilon \, \varepsilon^{\alpha \beta}(\boldsymbol{q}, \omega) = \delta^{\alpha \beta} + \frac{2}{\pi} \sum_{n \neq 0} \frac{(N_n^{\alpha \beta} + S_n^{\alpha \beta \gamma \delta} q_{\gamma} q_{\delta})}{E_n^2 - (\hbar \omega)^2}. \tag{2.19}$$

Taking into account all the symmetries from section 2.1 and comparing the result to the dielectric tensor from table 2.2

$$\varepsilon(\mathbf{q},\omega) = \varepsilon(\omega)\mathbb{1} + \gamma(\omega)|\mathbf{q}|^2 \begin{pmatrix} \hat{q}_1^2 & 0 & 0\\ 0 & \hat{q}_2^2 & 0\\ 0 & 0 & \hat{q}_3^2 \end{pmatrix}, \tag{2.20a}$$

$$\gamma(\omega)|\mathbf{q}|^2 \approx \gamma(\omega)\frac{\omega^2}{c^2}\varepsilon(\omega) = \varepsilon(\omega)p_1(\omega),$$
 (2.20b)

we can deduce the spectral functions. Recall, that  $\hat{q}$  is the unit vector in the direction of light propagation. We also defined the spectral function  $\gamma(\omega)$ , which is more practical than  $p_1(\omega)$  in terms of dispersion models. The reason is that we have to keep the wavevector and frequency dependence separated, since the Kramers-Kronig relations and sum rules are defined for a fixed value of the wavevector.

As mentioned previously,  $|q|^2 \approx n^2(\omega) \ \omega^2/c^2 \approx \varepsilon(\omega) \ \omega^2/c^2$ . The  $\varepsilon(\omega)$  and  $\gamma(\omega)$  functions are explicitly written as sum of Harmonic oscillators

$$\mathfrak{Re}\,\varepsilon(\omega) = 1 + \frac{2}{\pi} \sum_{n} \frac{N_{n}}{\omega_{n}^{2} - \omega^{2}}, \quad \mathfrak{Im}\,\varepsilon(\omega) = \sum_{n} \frac{N_{n}}{E_{n}} \,\delta(\hbar\omega - E_{n}),$$

$$\mathfrak{Re}\,\gamma(\omega) = \frac{2}{\pi} \sum_{n} \frac{S_{n}}{\omega_{n}^{2} - \omega^{2}}, \qquad \mathfrak{Im}\,\gamma(\omega) = \sum_{n} \frac{S_{n}}{E_{n}} \,\delta(\hbar\omega - E_{n}),$$
(2.21)

where n now denotes individual excitations, harmonic oscillators, with excitation energy  $E_n = \hbar \omega_n$ . The factor  $\hbar^{-2}$  was absorbed into the dimensionless constant  $S_n$ . The sum rules [26] applied to these functions read

$$\int_{0}^{\infty} d\omega \, \omega \mathfrak{Im} \varepsilon(\omega) = \sum_{n} N_{n} > 0,$$

$$\int_{0}^{\infty} d\omega \, \omega \mathfrak{Im} \gamma(\omega) = \sum_{n} S_{n} = 0.$$
(2.22)

#### 2.4 Berreman's formalism

Maxwell's equations represent a set of linear differential equations for the electromagnetic field. It is the property of linearity that allowed the american physicist D. W. Berreman to formulate a matrix formalism which describes the propagation of light through stratified anisotropic media. The formalism enables us to obtain reflection and transmission coefficients. At the same time, it presents a recipe on how to implement it in numerical computations.

Berreman, however, did not account for spatial dispersion, and so we need to make slight adjustments compared to the original work [20]. Additionally, we will show what to change in case of thick layers in which light from a real source cannot be assumed coherent anymore.

#### 2.4.1 Coherent multiple reflections

The original derivation starts with the macroscopic Maxwell's equations, in particular Ampére's and Faraday's laws, using the fields E, D, B, and H without any external sources. Then, constitutive relations are used to exclude the fields D and B. Note, that the formalism allows cross terms, called *optical-rotation tensors*, which are the proportionality constants for  $D \propto B$  and  $H \propto E$ . In our case there are no such cross terms, only the dielectric and permittivity tensors. So, for the sake of brevity, we shall omit them and also put  $\mu^{\alpha\beta}(\omega) = \delta^{\alpha\beta}$ .

We define the problem as restricted to the plane of incidence, say xz, with the surface normal oriented in the z direction. The main idea is to find eigenvectors that propagate inside individual layers, and then connect the fields at the interfaces. It can be shown, that the central equation is

$$\frac{\omega}{c} \begin{pmatrix}
-\hat{q}_{1} \frac{\varepsilon_{31}}{\varepsilon_{33}} & 1 - \hat{q}_{1}^{2} \frac{1}{\varepsilon_{33}} & -\hat{q}_{1} \frac{\varepsilon_{32}}{\varepsilon_{33}} & 0 \\
\varepsilon_{11} - \frac{\varepsilon_{13}\varepsilon_{31}}{\varepsilon_{33}} & -\hat{q}_{1} \frac{\varepsilon_{13}}{\varepsilon_{33}} & \varepsilon_{12} - \frac{\varepsilon_{13}\varepsilon_{32}}{\varepsilon_{33}} & 0 \\
0 & 0 & 0 & 1 \\
\varepsilon_{21} - \frac{\varepsilon_{23}\varepsilon_{31}}{\varepsilon_{33}} & -\hat{q}_{1} \frac{\varepsilon_{23}}{\varepsilon_{33}} & \varepsilon_{22} - \frac{\varepsilon_{23}\varepsilon_{32}}{\varepsilon_{33}} - \hat{q}_{1}^{2} & 0
\end{pmatrix} \begin{pmatrix}
E_{1} \\
H_{2} \\
E_{2} \\
-H_{1}
\end{pmatrix} = q_{3} \begin{pmatrix}
E_{1} \\
H_{2} \\
E_{2} \\
-H_{1}
\end{pmatrix}, (2.23)$$

where  $\hat{q}_1 = \sin(AOI)$  is the sine of the initial angle of incidence<sup>5</sup> which is constant across plane-parallel layers. The abbreviated form can be written as

$$\frac{\omega}{c} \Delta \psi = q_3 \psi. \tag{2.24}$$

Without spatial dispersion, the matrix  $\Delta$  is, at most, dependent on the *z*-coordinate, but constant over some finite interval  $(z_i, z_i + \delta_i)$  that represents one layer. The physical interpretation is that  $\Delta$  is the generator of translation of vector  $\psi$  in the *z*-direction

$$\psi(z_i + \delta_i) = e^{i\frac{\omega}{c}\delta_i \Delta(z)} \psi(z). \tag{2.25}$$

One then finds the solutions to the eigenproblem (2.24) and obtains four eigenvectors  $\psi_{\alpha}$  and corresponding eigenvalues  $q_{3,\alpha}$ , two of which are forward propagating modes  $q_{3,\alpha}>0$ , and two are backward propagating modes  $q_{3,\alpha}<0$ . It obvoiusly holds that  $\psi_{\alpha}(z_i+\delta_i)=\exp(i\omega\delta_i\,q_{3,\alpha}/c)\,\psi_{\alpha}(z)$ . The normalized eigenvectors can be stacked into a  $4\times 4$  matrix

$$\Psi = \left( \left( \psi_0 \right) \left( \psi_1 \right) \left( \psi_2 \right) \left( \psi_3 \right) \right). \tag{2.26}$$

This matrix  $\Psi$  can be thought of as a transformation into the basis of eigenmodes of the layer. The propagation through a layer of thickness d is governed by the matrix (cf. equation (2.25))

$$\mathbf{L}(d) = e^{i\frac{\omega}{c}d\Delta} = \mathbf{\Psi}\mathbf{K}(d)\mathbf{\Psi}^{-1}$$
, where  $\mathbf{K}^{\alpha\alpha}(d) = e^{i\frac{\omega}{c}d\,q_{3,\alpha}}$  (2.27)

is a diagonal matrix. For N layers, the total transfer matrix is calculated as

$$\Psi_{\text{out}}^{-1} \mathbf{L}_N(d_N) ... \mathbf{L}_1(d_1) \Psi_{\text{in}}.$$
 (2.28)

Usually,  $\Psi_{in} = \Psi_{out}$  are the vacuum solutions.

### A note on solving the eigenproblem with non-local response functions

When spatial dispersion is not neglected, the dielectric tensor  $\varepsilon(q,\omega)$  and hence the matrix  $\Delta$  depends not-trivially on the wavevector<sup>6</sup>. The eigenproblem (2.24) turns out to be a real problem because the characteristic polynomial

$$\det\left[\frac{\omega}{c}\Delta(\mathbf{q}) - q_3\mathbb{1}\right] = 0 \tag{2.29}$$

<sup>5.</sup> The initial medium is assumed to be vacuum. Otherwise it should be replaced by  $n_0 \sin(AOI)$  where  $n_0$  is the refractive index of the initial medium.

<sup>6.</sup> It definitely depends on frequency  $\omega$  as well, but this is of no importance here as everything is evaluated for a fixed value of  $\omega$ .

has now more than four solutions. A common approach is to impose additional boundary conditions (ABCs) that exclude some of the solutions. One of the first to introduce ABCs was Pekar in [18].

We will rather use a numerical approach where the issue of ABCs can be cleverly worked around. Observe, that spatial disersion may be treated as a perturbation and so for the unknown eigensolutions  $q_{\alpha}$  in the zeroth approximation  $\Delta(q_{\alpha}) \approx \Delta(0)$ . This is used to find the first approximate set of solutions  $q'_{\alpha}$  which are iteratively plugged back into  $\Delta(q'_{\alpha})$  and the eigenproblem (2.29) is again solved for a fixed  $\Delta$ . It has to be done for each of the four wavevectors  $q'_{\alpha}$  separately. Fortunately, the process separates into four independent branches, corresponding to four eigensolutions, which can be computed concurrently. The iteration is then repeated until a sufficient precision is achieved<sup>7</sup>. The process can be captured by a scheme 2.1.

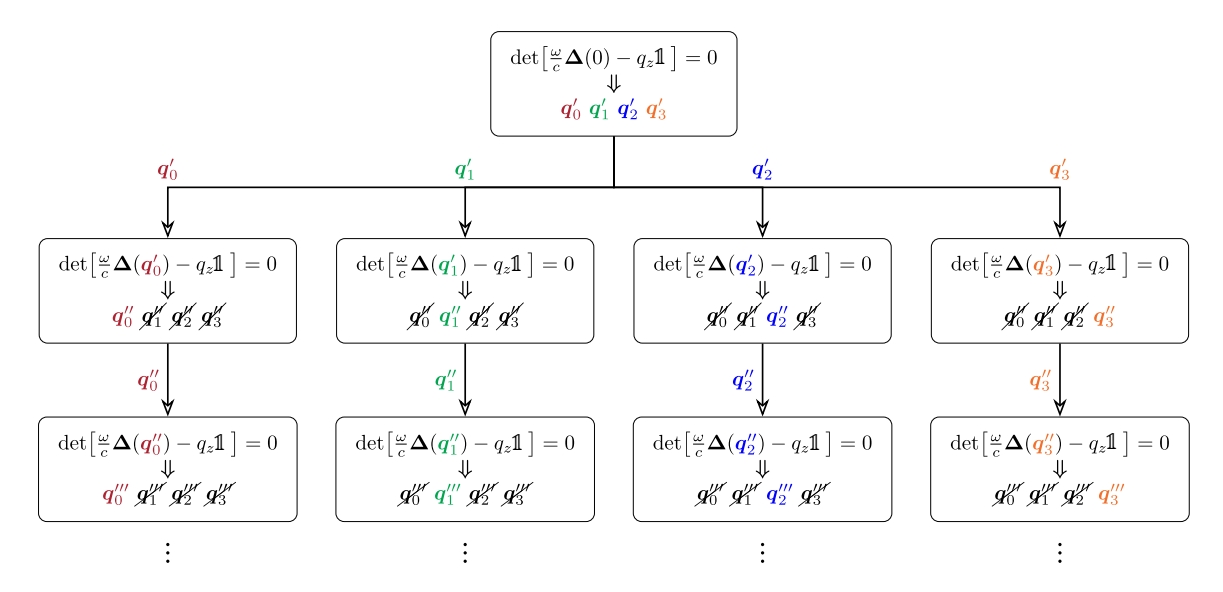


**Figure 2.1:** Scheme for iterative calculation of the  $\Delta$  matrix and its eigenvalues. It is assumed that the q-dependence is weak. We have stopped with  $q_n''$  in our calculations.

We are using only the first correction assuming that the wavevectos of eigenmodes are very close (in size as well as direction) to the ones computed for a local response. We would like to remind you, that for systems with cubic symmetry, the local response is isotropic. Therefore, after the first iteration, we get two doubly degenerate solutions, one for the forward travelling wave, and one for the backward. In the next iteration, we only have to solve the eigenproblem twice, but then obtain the four distinct solutions.

<sup>7.</sup> It is not certain if the algorithm will converge at all. Also, one has to be careful, once created the branches, not to replace  $q_{\alpha}$  in the  $\alpha^{\text{th}}$  branch by some different  $q_{\beta}$  during the computation process.

#### 2.4.2 Incoherent multiple reflections

When measuring layers with a thickness much bigger than the coherence length of the light source, the previous formalism is not suitable. A practical method was described for instance in [27-29].

The process goes as follows: First we separate the interface matrices and propagation matrices. Then each of them is decomposed into smaller  $2 \times 2$  matrices corresponding to forward/backward propagating modes and to reflected/transmitted modes. After that, these coherent reflection and transmission matrices are transformed into incoherent, so that when finally summing multiple reflections, the different parts of the beam do not interfere.

Starting with the total transfer matrix for a single layer of thickness d (cf. eqation (2.28)) and inverting it

$$\mathbf{\Psi}_{\text{in}}^{-1}\mathbf{L}(-d)\mathbf{\Psi}_{\text{out}},\tag{2.30}$$

where we have used the fact that  $\mathbf{L}^{-1}(d) = \mathbf{L}(-d)$  which is obvious from (2.27). For the following it is important that the eigenvalues are sorted so that the first two are forward propagating modes  $q_{3,\alpha} > 0$  for  $\alpha \in \{0,1\}$  and last two are backward propagating ones  $q_{3,\alpha} < 0$  for  $\alpha \in \{2,3\}$ .

We define three matrices that describe the boundary conditions

$$\mathbf{B}_{0,\text{fwd}} = \mathbf{\Psi}_{\text{in}}^{-1} \mathbf{L}(-d) = \begin{pmatrix} \left(\mathbf{B}_{00}^{0,\text{fwd}}\right) \left(\mathbf{B}_{01}^{0,\text{fwd}}\right) \\ \left(\mathbf{B}_{10}^{0,\text{fwd}}\right) \left(\mathbf{B}_{11}^{0,\text{fwd}}\right) \end{pmatrix},$$

$$\mathbf{B}_{0,\text{back}} = \mathbf{L}(d) \mathbf{\Psi}_{\text{in}} = \begin{pmatrix} \left(\mathbf{B}_{00}^{0,\text{back}}\right) \left(\mathbf{B}_{01}^{0,\text{back}}\right) \\ \left(\mathbf{B}_{10}^{0,\text{back}}\right) \left(\mathbf{B}_{11}^{0,\text{back}}\right) \end{pmatrix},$$

$$\mathbf{B}_{1,\text{fwd}} = \mathbf{L}(-d) \mathbf{\Psi}_{\text{out}}^{-1} = \begin{pmatrix} \left(\mathbf{B}_{00}^{1,\text{fwd}}\right) \left(\mathbf{B}_{01}^{1,\text{fwd}}\right) \\ \left(\mathbf{B}_{10}^{1,\text{fwd}}\right) \left(\mathbf{B}_{11}^{1,\text{fwd}}\right) \end{pmatrix},$$

$$(2.31)$$

where  $\mathbf{B}_{ij}$  are 2 × 2 submatrices and the indices "fwd" and "back" label the forward and backward travelling beams. The reflection and transmission dynamic matrices are a combination of these submatrices

$$\begin{split} \mathbf{T}_{0,\text{fwd}} &= \left(\mathbf{B}_{00}^{0,\text{fwd}}\right)^{-1}, \quad \mathbf{R}_{0,\text{fwd}} = \mathbf{B}_{10}^{0,\text{fwd}} \mathbf{T}_{0,\text{fwd}}, \\ \mathbf{T}_{0,\text{back}} &= \left(\mathbf{B}_{11}^{0,\text{back}}\right)^{-1}, \quad \mathbf{R}_{0,\text{back}} = \mathbf{B}_{01}^{0,\text{back}} \mathbf{T}_{0,\text{back}}, \\ \mathbf{T}_{1,\text{fwd}} &= \left(\mathbf{B}_{00}^{1,\text{fwd}}\right)^{-1}, \quad \mathbf{R}_{1,\text{fwd}} = \mathbf{B}_{10}^{1,\text{fwd}} \mathbf{T}_{1,\text{fwd}}, \end{split} \tag{2.32a}$$

and the propagation dynamic matrices  $P_{\text{fwd}}$  and  $P_{\text{back}}$  are connected to the diagonal matrix K(d) from (2.27) as

$$\mathbf{K}(d) = \begin{pmatrix} \left(\mathbf{P}_{\text{fwd}}^{-1}\right) \begin{pmatrix} \mathbf{0} \\ \mathbf{0} \end{pmatrix} \begin{pmatrix} \mathbf{P}_{\text{back}} \end{pmatrix} \end{pmatrix}. \tag{2.32b}$$

This means that the propagation dynamic matrices are diagoal as well with values on the diagonal correspondig to phase shifts of the forward and backward travelling modes.

So far, everything is coherent and the total coherent transmission T and reflection R matrices can be reconstructed by the classical geometric series that after summation give the result

$$T = T_{1,fwd} P_{fwd} \left[ 1 - R_{0,back} P_{back} R_{1,fwd} P_{fwd} \right]^{-1} T_{0,fwd},$$

$$R = R_{0,fwd} + T_{0,back} P_{back} R_{1,fwd} P_{fwd} \left[ 1 - R_{0,back} P_{back} R_{1,fwd} P_{fwd} \right]^{-1} T_{0,fwd}.$$
(2.33)

The trasformation to incoherent matrices is done by transitioning from the electromagnetic fields to description by intensities  $I \propto |E|^2$ . As a result, the information about the absolute phase is lost and different parts of light cannot interfere[19, 30]. A thorough derivation can be found in the book [31]. Here we merely list the transforming equations taken from this reference for the sake of completeness.

Each of the  $2 \times 2$  complex-valued dynamic matrices from equations (2.32) are mapped to the  $4 \times 4$  real valued so-called *Mueller matrices* **M** by the prescription for individual elements

$$\begin{split} M_{00} &= \frac{1}{2} \left( |D_{00}|^2 + |D_{01}|^2 + |D_{10}|^2 + |D_{11}|^2 \right) \\ M_{01} &= \frac{1}{2} \left( |D_{00}|^2 - |D_{01}|^2 + |D_{10}|^2 - |D_{11}|^2 \right) \\ M_{01} &= \frac{1}{2} \left( |D_{00}|^2 + |D_{01}|^2 - |D_{10}|^2 - |D_{11}|^2 \right) \\ M_{11} &= \frac{1}{2} \left( |D_{00}|^2 - |D_{01}|^2 - |D_{10}|^2 + |D_{11}|^2 \right) \\ M_{02} &= \mathfrak{Re} (D_{01} D_{00}^* + D_{11} D_{10}^*) \quad M_{20} = \mathfrak{Re} (D_{10} D_{00}^* + D_{11} D_{01}^*) \\ M_{03} &= -\mathfrak{Im} (D_{01} D_{00}^* + D_{11} D_{10}^*) \quad M_{30} = \mathfrak{Im} (D_{10} D_{00}^* + D_{11} D_{01}^*) \\ M_{12} &= \mathfrak{Re} (D_{01} D_{00}^* - D_{11} D_{10}^*) \quad M_{21} = \mathfrak{Re} (D_{10} D_{00}^* - D_{11} D_{01}^*) \\ M_{13} &= -\mathfrak{Im} (D_{01} D_{00}^* - D_{11} D_{10}^*) \quad M_{31} = \mathfrak{Im} (D_{10} D_{00}^* - D_{11} D_{01}^*) \\ M_{23} &= -\mathfrak{Im} (D_{11} D_{00}^* - D_{10} D_{01}^*) \quad M_{32} = \mathfrak{Im} (D_{11} D_{00}^* + D_{10} D_{01}^*) \\ M_{22} &= \mathfrak{Re} (D_{11} D_{00}^* + D_{10} D_{01}^*) \quad M_{33} = \mathfrak{Re} (D_{11} D_{00}^* + D_{10} D_{01}^*) \end{split}$$

for any dynamic matrix  $\mathbf{D}$ . We will denote the Mueller matrices corresponding to dynamic matrices in calligraphic font, for example  $\mathcal{D} = \mathbf{M}(\mathbf{D})$ . For the dynamic matrices

it holds that they are directly transformed,  $\mathcal{T}_{0,fwd} = M(T_{0,fwd})$ ,  $\mathcal{R}_{0,fwd} = M(R_{0,fwd})$ ,  $\mathcal{P}_{fwd} = M(P_{fwd})$ , and so on. But, in contrast with (2.33), the total transmission and reflection Mueller matrices are calculated as

$$\mathcal{T} = \mathcal{T}_{1,\text{fwd}} \mathcal{P}_{\text{fwd}} \left[ \mathbb{1} - \mathcal{R}_{0,\text{back}} \mathcal{P}_{\text{back}} \mathcal{R}_{1,\text{fwd}} \mathcal{P}_{\text{fwd}} \right]^{-1} \mathcal{T}_{0,\text{fwd}},$$

$$\mathcal{R} = \mathcal{R}_{0,\text{fwd}} + \mathcal{T}_{0,\text{back}} \mathcal{P}_{\text{back}} \mathcal{R}_{1,\text{fwd}} \mathcal{P}_{\text{fwd}} \left[ \mathbb{1} - \mathcal{R}_{0,\text{back}} \mathcal{P}_{\text{back}} \mathcal{R}_{1,\text{fwd}} \mathcal{P}_{\text{fwd}} \right]^{-1} \mathcal{T}_{0,\text{fwd}}.$$
(2.35)

Clearly, the mapping (2.34) does not preserve linearity and hence  $\mathcal{T} \neq M(T)$ , and  $\mathcal{R} \neq M(R)$ .

Finally, we would like to point out, that a surface layer with coherent multiple reflections can be simply added by substituing  $\Psi_{\rm in} \to \Psi_{\rm in} \mathbf{L}_\ell(d_\ell)$ , where  $\mathbf{L}_\ell(d_\ell)$  is the propagation matrix of the layer with thickness  $d_\ell$ . An analogous substitution can be made for the back side  $\Psi_{\rm out} \to \Psi_{\rm out} \mathbf{L}_\ell(d_\ell)$ .

### 2.4.3 No multiple reflections

Sometimes, there is a need to completely remove higher-order reflections from the calculations. This may happen if the light gets absorbed so that the second- and next-order reflections are orders of magnitude weaker than the primary signal. Another possibility is that the beam is refracted and deviated, so that it does not hit the detector slit. This occurs mainly when measuring thick samples with a large refractive index at a large *AOI* [28].

In this case, the transmission and reflection matrices become

$$T = T_{1,\text{fwd}} P_{\text{fwd}} T_{0,\text{fwd}},$$

$$R = R_{0,\text{fwd}},$$
(2.36)

and for Mueller matrices

$$\mathcal{T} = \mathcal{T}_{1,\text{fwd}} \mathcal{P}_{\text{fwd}} \mathcal{T}_{0,\text{fwd}},$$

$$\mathcal{R} = \mathcal{R}_{0,\text{fwd}}.$$
(2.37)

Note that the map  $M(\cdot)$  from (2.34) preserves matrix multiplication<sup>8</sup> and therefore it now holds that  $\mathcal{T}=M(T)$  and  $\mathcal{R}=M(R)$ .

Finally, we would like to emphasize that the main advantage of Mueller matrices is that they are operating on light intensities  $I \propto |E|^2$ , which can be easily directly measured as opposed to the quickly varying electric and magnetic field intensities used in Berreman formalism.

<sup>8.</sup> The transformation to Mueller matrices can be written as  $\mathbf{M}(\mathbf{D}) = \mathbf{A}(\mathbf{D} \otimes \mathbf{D}^*) \mathbf{A}^{-1}$ , where  $\mathbf{A}$  is some constant unitary matrix and the symbol " $\otimes$ " denotes the *Kronecker product* [27, 29]. Despite the Kronecker product being a bilinear map, the map  $\mathbf{M}(\cdot)$  is not linear. It holds, however, that  $(\mathbf{A} \otimes \mathbf{B})(\mathbf{C} \otimes \mathbf{D}) = (\mathbf{AC}) \otimes (\mathbf{BD})$  for any matrices  $\mathbf{A}$ ,  $\mathbf{B}$ ,  $\mathbf{C}$ , and  $\mathbf{D}$  [28]. Hence,  $\mathbf{M}(\cdot)$  preserves multiplication.

# 3 Experimental methods

This chapter aims to provide details of the experiments that we have carried out. We employed Mueller matrix ellipsometry (polarimetry). Therefore, the first section is a brief introduction into the Mueller calculus.

In the second section, we explain the experimental setup of the reflection and transmission measurements and introduce the instruments used. All presented measurements were performed in the optical laboratory at the University of Barcelona.

In the last part we report technical parameters about samples that were used in the study.

#### 3.1 Mueller matrices

In chapter 2, we briefly mentioned Mueller matrices. They mediate the transformations between two intensity vectors, also called the *Stokes vectors*, defined as

$$S = \begin{pmatrix} I_{\text{tot}} \\ I_x - I_y \\ I_{45} - I_{135} \\ I_R - I_L \end{pmatrix}. \tag{3.1}$$

Its elements are time-averaged intensities of different polarizations [19]. The orientations subscripts x, y,  $45^{\circ}$ , and  $135^{\circ}$  mark intensities of linearly polarized light in the given direction w.r.t. the coordinate axes. Subscripts L and R denote left- and right-handed circular polarizations. Finally,  $I_{\text{tot}}$  is the total intensity, for which it holds that  $I_{\text{tot}}^2 \leq (I_x - I_y)^2 + (I_{45} - I_{135})^2 + (I_R - I_L)^2$ . The equality is satisfied if the light is completely polarized.

In practice, Mueller matrices are mostly used to represent optical elements of some experimental setup, especially measured samples. The change of the incoming light described by a Stokes vector  $S_{in}$  to the outgoing light  $S_{out}$  is written as

$$S_{\text{out}} = \mathbf{M}S_{\text{in}}.\tag{3.2}$$

Often, however, we are rather interested in the properties of the material, not the sample as a whole. In this case, it is preferable to use the differential Mueller matrix [32–34], which we will denote as **m**. It is defined as the matrix logarithm of the Mueller matrix. The differential Mueller matrix has seven unique elements if the material is non-depolarizing [34, 35],

$$\mathbf{m} = \log \mathbf{M} = \begin{pmatrix} -\kappa & -LD & -LD' & CD \\ -LD & -\kappa & CB & LB' \\ -LD' & -CB & -\kappa & -LB \\ CD & -LB' & LB & -\kappa \end{pmatrix}.$$
(3.3)

The meaning of the individual elements is captured in the table 3.1. Note, that the elements have a meaning only for bulk propagation [36]. Nevertheless, it is possible to define analogous quantities for the entire sample too.

**Table 3.1:** Elements of the differential Mueller matrix (3.3).  $\lambda$  is the wavelength, d the path length in a medium, n is the refractive index, k the extinction coefficient. The subscripts x, y, 45, and 135 stand for directions of linar polarizations w.r.t. the coordinate system. L and R denote left- and right-handed circular polarization, respectively. Definitions are taken from [36, 37].

The isotropic amplitude absorption describes the decrease of the overall intensity  $I_{\rm tot}$ . The birefringences describe the phase shift (different propagation speed) of two orthogonal polarizations. Finally, the dichroisms express the difference of attenuations of two orthogonal polarizations. Clearly, if the material is completely non-absorbing, its differential Mueller matrix can have only three elements different from zero, the birefringences.

Another special case is when the studied material does not exhibit optical activity or any kind of gyrotropy. Then, circular birefringence is zero. Hence, when dealing with cubic crystals from the crystallographic groups  $m\bar{3}m$ ,  $\bar{4}3m$ , and  $m\bar{3}$  in the absorption-free wavelength range, only the linear birefringences LB and LB' are of interest.

In the absence of absorption and gyrotropy, the (*linear*) retardance (LR) is given by  $LR = \sqrt{LB^2 + LB'^2}$ . If the reference frame coincides with the optic axis, it expresses the difference of the refractive indices of the ordinary and extraordinary waves [36]. The linear retardance of achiral cubic crystals is shown in figure 3.1. We can clearly see the four-fold symmetry of the [001] direction and the three-fold symmetry of the [111] direction. Moreover, there is no birefringence in these two directions, and the maximum retardance is in the [011] direction.

For completeness, we are showing also the directional dependence and projections of LR in the case of the less symmetric group  $m\bar{3}$  in figure 3.2. Clearly, the drection

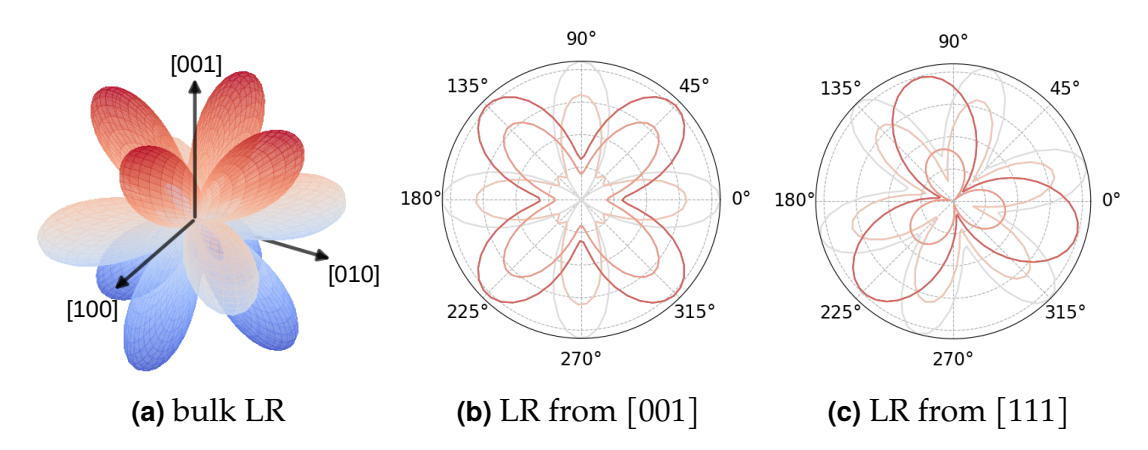


**Figure 3.1:** Linear retardance (LR) due to spatial dispersion of a crystal belonging to the  $m\bar{3}m$  or  $\bar{4}3m$  crystallographic groups. (a) is the directional dependence of the LR inside the crystal. The mapping of LR viewed from the direction [001] for constant values of  $\cos(AOI)$  is depicted in (b). The same, but viewed from the direction [111] is in (c).

[001] has a lower (two-fold) symmetry compared to the groups  $m\bar{3}m$  and  $\bar{4}3m$ . The lacking symmetry is the reason why the dielectric tensor of group  $m\bar{3}$  depends on two parameters.

## 3.2 Spectroscopic polarimetry

The main principle of ellipsometry/polarimetry is to measure the polarization of light that is reflected from or propagated through the sample. For that, we need a light source with an optical system that is capable of creating different polarizations, and a light detector that has an optical system for analyzing light polarizations. Depending on the ability of the polarization state generator (PSG) and the polarization state analyzer (PSA), different combination of the Mueller matrix components can be measured.

The simplified experimental setup is shown in figure 3.3, and is common to all our transmission measurements. The PSG generates light with a well-defined polarization state. It travels through the sample where it gets reflected and refracted, so its polarization state changes. The change is then analyzed by the PSA. As we mentioned in section 3.1, there is no birefringence in the [001] and [111] directions. However, if the sample with one of these two surface orientations is tilted, then the linear retardance (LR) becomes finite. Rotating the sample around its surface normal, *i. e.* around the four- and three-fold symmetric axis, the LR shows the respective symmetry.

In our study, we used two home-built instruments which measure the complete Mueller matrix. Both have the PSG and the PSA composed of a polarizer and a compensator. The first of them utilizes Fresnel rhombs as compensators, and we will label

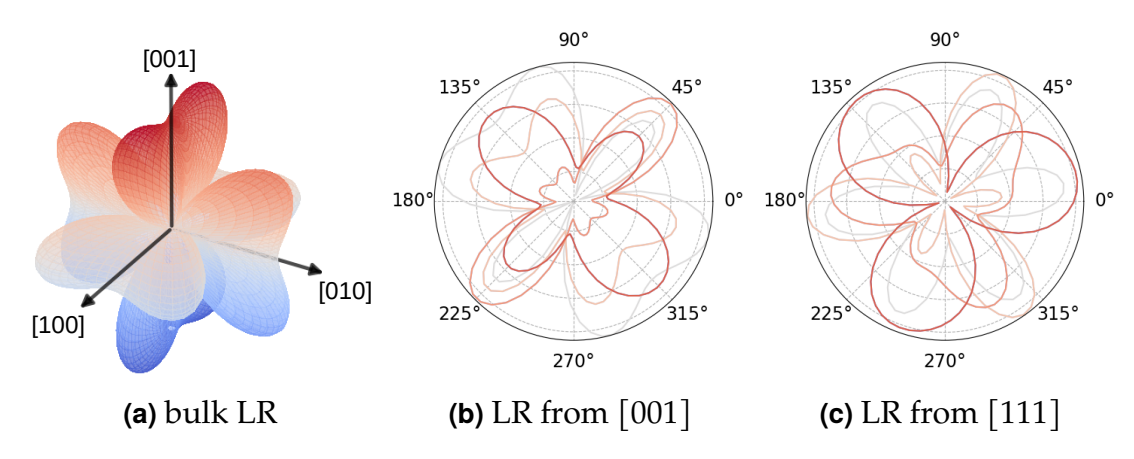


**Figure 3.2:** Linear retardance (LR) due to spatial dispersion of a crystal belonging to the  $m\bar{3}$  crystallographic group. The ratio of the parameters defining the SD tensor was chosen as  $p_2/p_1=0.6$ . (a) is the directional dependence of the LR inside the crystal. The LR viewed from the direction [001] for fixed values of  $\cos(AOI)$  is depicted in (b). The same, but viewed from the direction [111] is in (c).

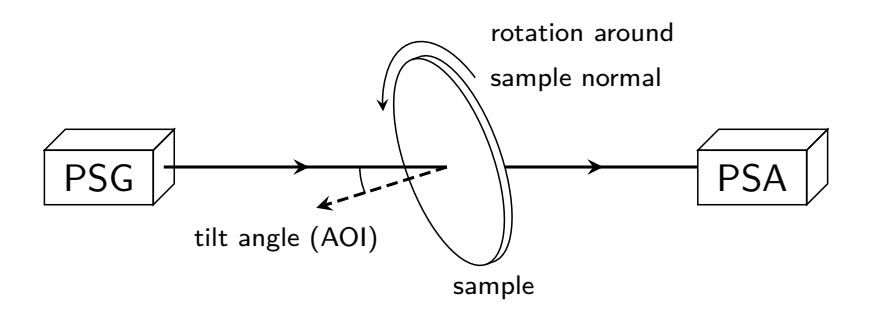


**Figure 3.3:** Basic polarimetric cofiguration of transmission measurements. PSG is the polarization state generator, and PSA is the polarization state analyzer.

the istrument as FRE. We used it fr spectral transmission measurements in the infrared range where the upper wavelenght limit 1150 nm is restricted by the CCD spectrometer. For further details see [38].

The second instrument has compensators composed of two photoelastic modulators on each side, hence we will call it 4PEM. It was used in the near ultraviolet transmission measurements and for reflection measurements in [17]. More about this instrument can be found in [39, 40].

### 3.3 Samples

All the samples with their characteristics, and the instruments used in this study are listed in table 3.2. We measured samples made of silicon (Si) and calcium fluoride

**Table 3.2:** Experimental data information. Measurements were performed in transmission (T) and reflection (R). In the case of transmission, refractive index (RI) data were taken from the indicated literature. In the case of reflection measurement, the processed data were provided by the authors of the cited article. All Si samples are double side polished.

material	surface orientation	thickness $[\mu m]$	experiment type	instrument	wavelength (range) [nm]	RI/data source
Si	(001)	525(5)	Т	FRE	1000	[23]
Si	(111)	404(5)	T	FRE	1000	[23]
Si	(011) <sup>†</sup>	503(5)	T	FRE	(995, 1490)	[23]
	(011)	303(3)	R	4PEM	(190, 799)	[17]
CaF <sub>2</sub>	(111)	500	T	4PEM	260	[41]

<sup>†</sup> In the transmission measurement 20 samples were measured.

 $(CaF_2)$ . Both crystals are cubic and belong to the  $m\bar{3}m$  point group. The silicon wafers are all double side polished and the  $CaF_2$  sample is a  $5\times 5$  mm square monocrystal. Their thicknesses were measured using a micrometer. The presented Si (001) wafer and  $CaF_2$  thicknesses were taken from the manufacturer. In the case of Si (011) we made an average of 20 samples with the same nominal thickness, therefore, also an average thickness was used.

We performed the polarimetric measurements in tranmission (T). The ellipsometric reflection measurements (R) were made and analyzed by Bian *et. al.* [17]. In our analysis we used the average refractive index from literature [23, 41].

### 4 Results and discussion

This chapter reports the results of our analysis and is divided into two parts. The first one discusses the spectral dependence of spatial dispersion, where we have tested our proposed dispersion model on experimental data. The second one deals with the spatial variation of the measured linear birefringence, which, due to the symmetry, clearly originates in spatial dispersion.

In the ideal case, experimental Mueller matrices coincide with the Mueller matrix of the sample  $\mathbf{M}_s$ . However, in reality there is also a response from the PSG and PSA optics ( $\mathbf{M}_G$  and  $\mathbf{M}_A$ ), that cannot be always totally elliminated by callibration. The real measurement gives the measurable quantity is  $\mathbf{M}_{tot}$ ,

$$\mathbf{M}_{\text{tot}} = \mathbf{M}_{\mathbf{A}} \mathbf{M}_{\mathbf{S}} \mathbf{M}_{\mathbf{G}}.\tag{4.1}$$

With each measurement, we made an additional measurement without a sample ("background measurement"), that gives the instrument response

$$\mathbf{M}_{\mathrm{I}} = \mathbf{M}_{\mathrm{A}} \mathbf{M}_{\mathrm{G}}.\tag{4.2}$$

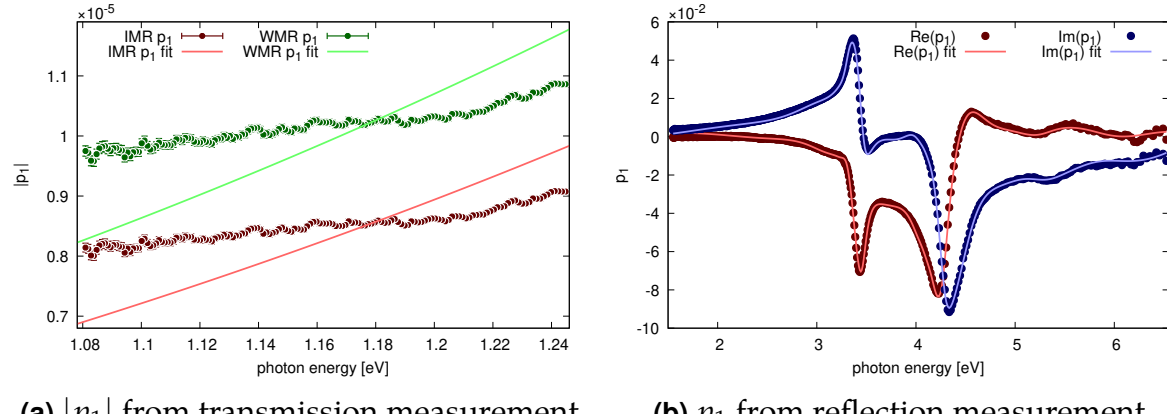
Evidently, in general, we are not able to directly assess  $M_S$ . However, if we assume that the matrices of the instrument are close to identity and that they approximately commute, then we might express the differential Mueller matrix (3.3) of the sample in terms of  $M_{tot}$  and  $M_I$ ,

$$\begin{aligned} \mathbf{m}_{\mathrm{S}} &= \log \left( \mathbf{M}_{\mathrm{A}}^{-1} \mathbf{M}_{\mathrm{tot}} \mathbf{M}_{\mathrm{G}}^{-1} \right) \\ &\approx \log \mathbf{M}_{\mathrm{tot}} - \log \mathbf{M}_{\mathrm{A}} - \log \mathbf{M}_{\mathrm{G}} \\ &\approx \log \mathbf{M}_{\mathrm{tot}} - \log \mathbf{M}_{\mathrm{I}}. \end{aligned} \tag{4.3}$$

This correction was made for all our presented measurements. In the case of transmission, we have assumed that the dielectric tensor is real-valued.

### 4.1 Spectral analysis

Twenty silicon wafers with surface orientation (011) were measured in transmission at normal incidence using the FRE in the wavelength range (995, 1490) nm. The experimental Mueller matrices were processed and the obtained birefringences LB and LB' were translated into  $LR = \sqrt{LB^2 + LB'^2}$ . This quantity was fitted for each wavelength separately with the form of the response tensors from table 2.2, taking into account incoherent multiple reflections inside the sample. From this, we were able to get the absolute value of the  $p_1$  parameter as a function of wavelength.



- (a)  $|p_1|$  from transmission measurement
- **(b)**  $p_1$  from reflection measurement

**Figure 4.1:** The parameter  $p_1$  obtained from measurements of slicon in the transparent region with multiple reflections calculated incoherently (IMR), and disregarding multiple reflections (WMR) and fitted with the two-term harmonic oscillator model (a). The real and imaginary parts of  $p_1$  from reflection measurement fitted with the Universal dispersion model (b).

The refractive index of silicon in the transparent region can be described by a twoterm Sellmeier formula with great accuracy. The same applies to the real part of the permittivity function  $\Re \varepsilon(\omega)$ . We used this fact and extended the classical Sellmeier formula to the modified harmonic oscillator model presented in section 2.3. Assuming real functions, the dispersion model from combining (2.21) and (2.20b) with two excitations is

$$\varepsilon(E) = 1 + \frac{2}{\pi} \left[ \frac{N_1}{E_1^2 - E^2} + \frac{N_2}{E_2^2 - E^2} \right],$$

$$p_1(E) = \frac{2}{\pi} \left[ \frac{SE^2}{E_1^2 - E^2} - \frac{SE^2}{E_2^2 - E^2} \right],$$
(4.4)

where we have already made use of the sum rule for the transition strengths  $\sum_{n} S_n = 0$ (see equation (2.22)), and absorbed the factor  $\hbar^2$  into  $N_n$  and S. The result is shown in figure 4.1. The fitted value is  $S = -(1.5021 \pm 0.0006) \cdot 10^{-4}$  for the incoherent multiple reflection model and  $S = -(1.7981 \pm 0.0007) \cdot 10^{-4}$  in case of the model without multiple reflections. We see that the modified harmonic oscillator model does not faithfully capture the dispersion of  $p_1$ . Reasons for the discrepancy may range from improper callibration to an oversimplified model. As for now, we have not resolved tis issue.

Subiao Bian kindly provided us with the reflection data of silicon (011) published in [17]. We fitted them simultaneously with the optical constants using the software newAD2 [42]. The optical constants from far infrared to vacuum ultraviolet (0.01 -10 eV) were generated using the Advanced dispersion model at room temperature [43]. They were fitted with the Universal dispersion model with a splitted bandgap using two effective phonons [23]. This way we were able to precisely describe the indirect band gap of crystalline silicon. The interbnd electron excitations were modeled by a combination of Gaussian peaks and the Campi-Coriosso model. In addition, we used a model of the Urbach tail for the subgap absorption. Multiphonon excitations were modeled by Gaussian peaks. Spatial dispersion was considered only for electron interband excitations.

## 4.2 Spatial analysis

The spatial dependence of linear retardance was measured in transmission mode as indicated in figure 3.3. The azimuthal rotation of the sample around its normal is fully automatized. Silicon samples were measured at the wavelength 1000 nm, using the FRE at different angles of incidence. The upper limit of the angle of incidence is given by the sample holder.

We have already mentioned, that linear retardance of the  $m\bar{3}m$  group has the largest magnitude in the direction [011] (see section 3.1 and figures therein). We measured 20 wafers of Si (011) and by fitting the linear retardance we obtained the value of  $|p_1|$ . Clearly, it is model-dependent. In our study, we have first tried the model which accounts for multiple reflections summed incoherently, and then tried the model that takes only the primary (non-reflected) beam. The completely coherent model is in our case inapplicable, as the ratio sample thickness/wavelength is too big and the interference pattern cannot be resolved. The first model yields  $|p_1| = (9.066 \pm 0.038) \cdot 10^{-6}$ . From the second model, we got a slightly bigger value of  $|p_1| = (1.085 \pm 0.005) \cdot 10^{-5}$ .

The effects of the surface layer is significant at oblique angles, in contrast to normal incidence. We measured the thickness of the silicon oxide layer by reflection ellipsometry on the FRE and with the help of the WVASE software [44]. The results are presented in table 4.1. It was not possible to fit the experimental data of Si (001) and Si (111)

**Table 4.1:** Measured thicknesses of the native silicon oxide layer of both sides of the used samples. Values were obtained by reflection ellipsometry.

	Si (001)	Si (011)	Si (111)
front	2.2(4) nm	2.4(7) nm	2.5(4) nm
back	2.3(4) nm	1.8(2) nm	3.8(7) nm

measured at oblique AOI without accounting the surface layer. We added a coherent  $SiO_2$  layer as indicated in section 2.4.2. It simulates the native layer on both sides of the sample, and assumes the same, but variable thickness.

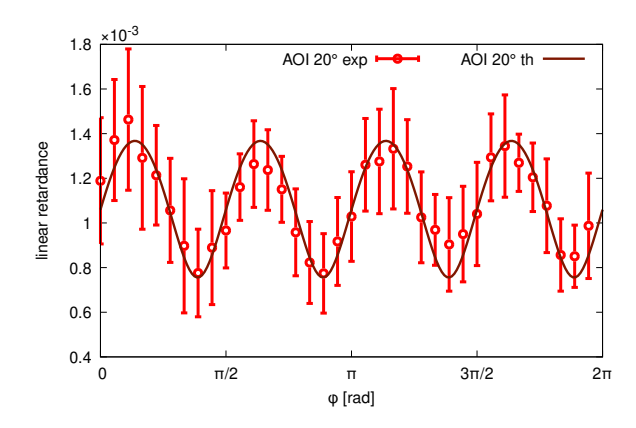


**Figure 4.2:** Linear retardance at 1000 nm of silicon with surface orientation (001) measured at angle of incidence  $20^{\circ}$ . Data are fitted with the model of incoherent multiple reflections. The  $p_1$  value was fixed from the Si (011) measurement. The fitted value of the native oxide layer is  $(3.843\pm0.065)$  nm.

**Table 4.2:** Values of fitted parameters and the  $\chi^2$  for comparisson of two models: the incoherent multiple reflection (IMR), and the model without multiple reflections (WMR).

sample	model	$ p_1 $	SiO <sub>2</sub> thickness	$\chi^2$
Si (011)	IMR WMR	$(9.066 \pm 0.037) \cdot 10^{-6}$ $(1.085 \pm 0.005) \cdot 10^{-5}$	N/A	182.307399 182.307401
Si (001)	IMR WMR	N/A	$(3.843 \pm 0.065)  \mathrm{nm}$ $(3.842 \pm 0.066)  \mathrm{nm}$	5.3825 5.2953
Si (111)	IMR WMR	N/A	$(2.99 \pm 0.30)  \mathrm{nm}$ $(2.80 \pm 0.31)  \mathrm{nm}$	14.869 14.909
CaF <sub>2</sub> (111)	IMR WMR IMR <sup>†</sup> WMR <sup>†</sup>	$ \begin{array}{c} (2.66 \pm 0.09) \cdot 10^{-7} \\ (2.68 \pm 0.08) \cdot 10^{-7} \\ -(2.408 \pm 0.071) \cdot 10^{-7} \\ -(2.371 \pm 0.072) \cdot 10^{-7} \end{array} $	N/A	19.588 19.612 92.224 91.878

<sup>†</sup> In this case we fitted directly LB and LB', so we are sure  $p_1$  has the correct sign.

When fitting the surface layer thickness, it correlates significantly with the  $p_1$  value. At normal incidence, there is practically no effect of the layer. So we used the previously obtained  $p_1$  value from Si (011), and tried to fit only the SiO<sub>2</sub> thickness. The results for the model of incoherent reflections are shown in figures 4.2 and 4.3.

The model without multiple reflections gives almost the same results. We provide a numerical comparisson in table 4.2. We were not able to find any literature for comparing the silicon measurements.

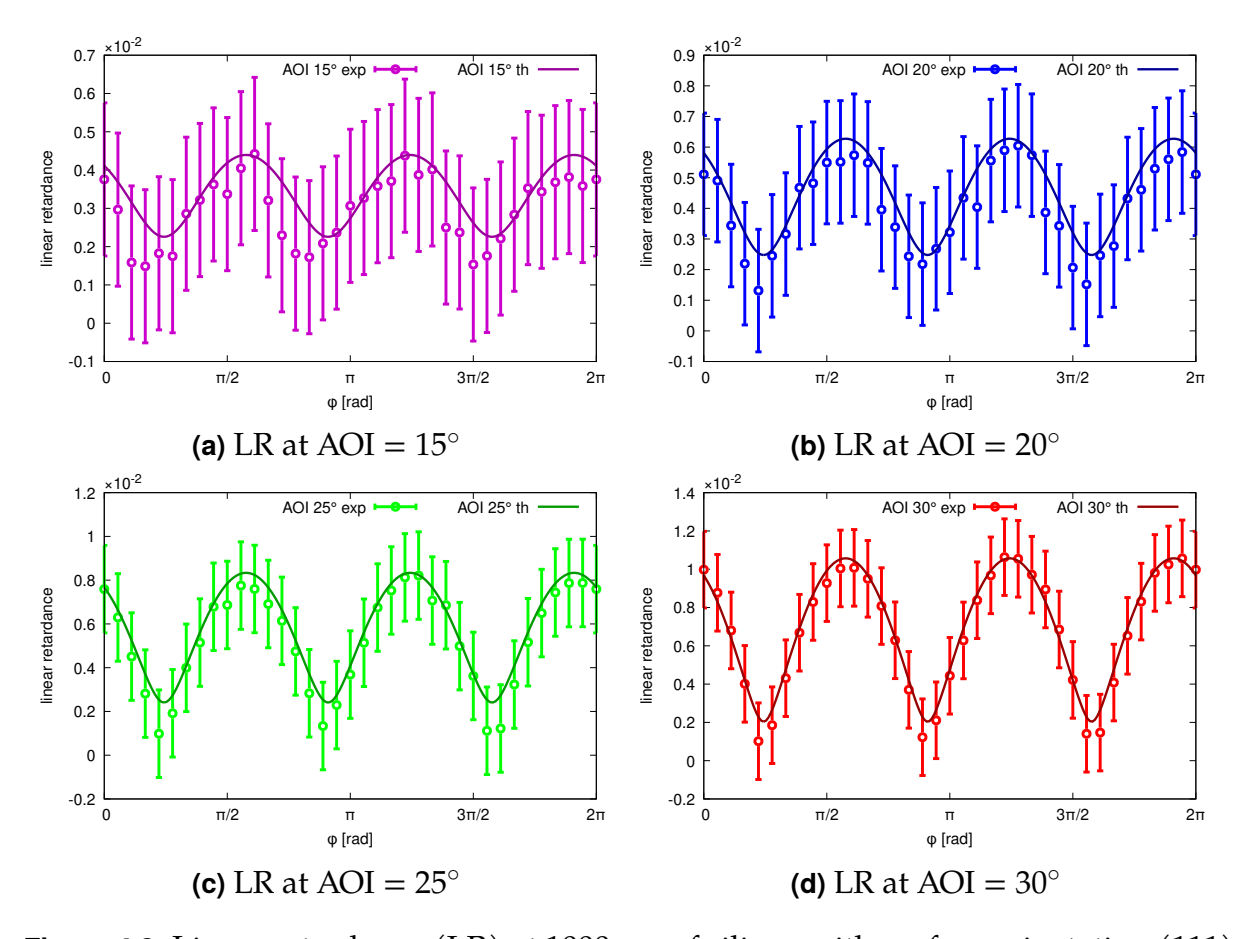


**Figure 4.3:** Linear retardance (LR) at 1000 nm of silicon with surface orientation (111) measured at an angle of incidence (AOI) (a)  $15^{\circ}$ , (b)  $20^{\circ}$ , (c)  $15^{\circ}$ , and (d)  $30^{\circ}$ . Experimental data are fitted with the model of incoherent multiple reflections. The  $p_1$  value was taken from normal incidence measurement of (011) silicon. The fitted value of the native oxide layer is  $(2.98 \pm 0.30)$  nm.

The calcium fluoride sample was measured at the wavelength 260 nm using the 4PEM. We had only one sample available with the orientation (111). Compared to silicon,  $CaF_2$  has no native surface layer. It shows, however, a significantly smaller birefringence. We can see from the results, that the three-fold symmetry of the LR is no longer visible.

The difference of refractive indices  $\Delta n = n_{<0.11>} - n_{<0.01>}$  for CaF<sub>2</sub> was reported by Burnett *et. al.* [1]. At the wavelength 253.65 nm they measured  $\Delta n = -(0.55 \pm 0.07) \cdot 10^{-7}$ . In our case the difference can be obtained from  $p_1$  as

$$\Delta n = n\sqrt{1 + p_1} - n. \tag{4.5}$$

Taking the last two results from 4.2, where directly *LB* and *LB'* were fitted, we ged the refractive index difference at the wavelength 260 nm as  $\Delta n = -(1.763 \pm 0.052) \cdot 10^{-7}$  for the IMR model and  $\Delta n = -(1.953 \pm 0.053) \cdot 10^{-7}$  for the WMR model.

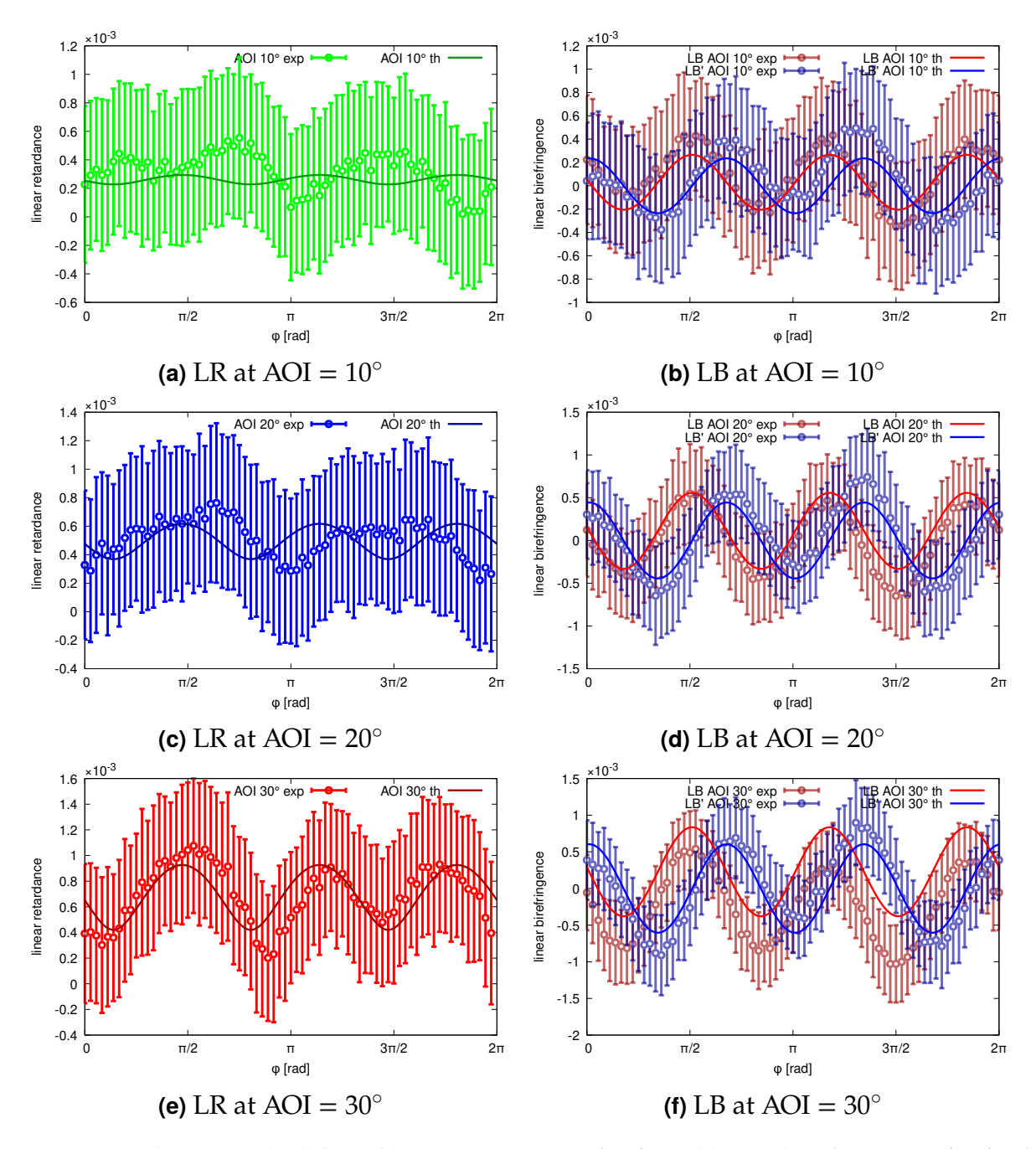


**Figure 4.4:** The individual fits of linear retardance (LR) and linear birefringence (LB) of a CaF<sub>2</sub> sample at 260 nm. The angle of incidence is  $10^{\circ}$  in (a) and (b),  $20^{\circ}$  in (c) and (d),  $30^{\circ}$  in (e) and (f). Experimental data corresponding to one AOI are the same, but fitted at different levels.

### 5 Conclusion

We derived the dielectric tensor as a linear response function to the external electromagnetic field. We showed how spatial disprsion emerges from the multipole expansion of the vector potential.

We chose cubic crystals for a closer study because, without spatial dispersion (SD), they have an isotropic response and have no intrinsic birefringence which would make it significantly harder to measure the weak birefringence comming from SD. In particular, achiral cubic crystals are of our interest since the dielectric tensor contains no term odd in the components of the wavevector, *i. e.* there is no gyrotropy. We showed that in the limit of weak SD ( $|q|a \ll 1$ , where a is a characteristic spatial dimension), the wavevector-dependent dielectric tensor depends only on one (classes  $m\bar{3}m$ ,  $\bar{4}3m$ ) or two (class  $m\bar{3}$ ) additional parameters, the spectral functions  $p_1(\omega)$  and  $p_2(\omega)$ .

We have presented a method for reformulation of the response functions can be reformulated so that no additional boundary conditions need to be imposed. This was used to derive the  $4\times 4$  Berreman matrix formalism for light propagation. We emphasized the differences between the usual formalism and the one modified for spatial dispersion.

We introduced a dispersion model that is an analogue of the Harmonic oscillator model, (Sellmeier formula), commonly used in the transparent spectral region. We have tested the proposed model on experimental data from a double side polished silicon wafer. The theoretical functions show a steeper dispersion than we have obtained from polarimetric measurements of birefringence 4.1. On the other hand, we were able to fit the spectral functions from reflection measurements by employing a similar modification of the Universal dispersion model as we did for the Harmonic oscillator.

Concerning the directional dependence of SD, we successfully measured the threeand the four-fold symmetry of the crystallographic directions [001] and [111], respectively. We focused on studying how multiple reflections affect the value of the parameter  $p_1$ , and how it is affected by the native oxide layer on the silicon surface. Although there are no significant differences when accounting for multiple relections inside the sample or discounting all reflections, we incline to the model with incoherent reflections.

The oblique angle measurements of  $CaF_2$  give very weak response in agreement with our expectations. For the silicon we still cannot explain the discrepancy between the theory and experiment. Silicon is slightly more challenging because (a) there is a native oxide layer that does affect the birefringence, and (b) the refractive index of silicon is relatively high, which requires a large angle of incidence to deviate from the isotropic directions [001] or [111].

There is no doubt that our experiments measure SD, since no other effect can result in a three- and four-fold symmetric anistropy in the linear retardance. At this point, we cannot prove our theory wrong. There are still many things that deserve more attention.

# **Bibliography**

- [1] J. Burnett, Z. Levine, E. Shirley, and J. Bruning, "Symmetry of Spatial-Dispersion-Induced Birefringence and its Implications for CaF2 Ultraviolet Optics", *Journal of Micro/Nanolithography*, MEMS, and MOEMS, vol. 1, 2002, por: 10.1117/1.1503350.
- [2] V. G. Vladimir M. Agranovich, *Crystal Optics with Spatial Dispersion, and Excitons* (Springer Series in Solid-State Sciences), 2nd ed. Berlin: Springer-Verlag Berlin, 1984, DOI: 10.1007/978-3-662-02406-5.
- [3] J. Pastrnak and K. Vedam, "Optical Anisotropy of Silicon Single Crystals", *Phys. Rev. B*, vol. 3, pp. 2567–2571, 8, 1971, DOI: 10.1103/PhysRevB.3.2567.
- [4] T. Chu, M. Yamada, J. Donecker, M. Rossberg, V. Alex, and H. Riemann, "Optical anisotropy in dislocation-free silicon single crystals", *Microelectronic Engineering*, vol. 66, no. 1, pp. 327–332, 2003, Proceedings of the 8th International Conference on Electronic Materials (IUMRS-ICEM2002), ISSN: 0167-9317, DOI: https://doi.org/10.1016/S0167-9317(02)00935-8.
- [5] J. H. Burnett, Z. H. Levine, and E. L. Shirley, "Intrinsic birefringence in calcium fluoride and barium fluoride", *Phys. Rev. B*, vol. 64, p. 241102, 24, 2001, DOI: 10.1103/PhysRevB.64.241102.
- [6] L. D. Landau, E. M. Lifsits, J. S. Bell, M. J. Kearsley, L. P. Pitaevskij, and J. B. Sikes, *Electrodynamics of Continuous Media*, 2nd ed. Pergamon Press, 1984, ISBN: ISBN: 9780080302751.
- [7] M. E. Peskin and D. V. Schroeder, *An Introduction to Quantum Field Theory*. Westview Press, 1996, DOI: 10.1063/1.2807734.
- [8] G. D. Mahan, *Many-particle physics*. Springer Science & Business Media, 2013, DOI: 10.1007/978-1-4757-5714-9.
- [9] A. L. Fetter and J. D. Walecka, *Quantum theory of many-particle systems* (International series in pure and applied physics). New York, NY: McGraw-Hill, 1971, DOI: 10.1063/1.3071096.
- [10] N. Zettili, Quantum Mechanics: Concepts and Applications, 2nd ed. United Kingdom: John Wiley & Sons, 2009, ISBN: 978-0-470-02678-6.
- [11] J. Skaar, H. O. Hågenvik, and C. A. Dirdal, "Four definitions of magnetic permeability for periodic metamaterials", *Phys. Rev. B*, vol. 99, p. 064 407, 6, 2019, DOI: 10.1103/PhysRevB.99.064407.
- [12] A. C. Sharma and S. Auluck, "Transverse dielectric function for a model semiconductor", *Phys. Rev. B*, vol. 24, pp. 4729–4735, 8, 1981, DOI: 10.1103/PhysRevB.24.4729.
- [13] D. Franta and J. Vohánka, "Constitutive equations describing optical activity in theory of dispersion", *J. Opt. Soc. Am. B*, vol. 38, no. 2, pp. 553–561, 2021, DOI: 10.1364/JOSAB.410315.

- [14] R. Ossikovski, O. Arteaga, and C. Sturm, "Constitutive Relations for Optically Active Anisotropic Media: A Review", *Advanced Photonics Research*, vol. 2, no. 12, p. 2100160, 2021, DOI: https://doi.org/10.1002/adpr.202100160.
- [15] R. Ossikovski and O. Arteaga, "Optical response of media and structures exhibiting spatial dispersion", *Opt. Lett.*, vol. 47, no. 21, pp. 5602–5605, 2022, DOI: 10.1364/0L.475069.
- [16] J. F. Nye, *Physical Properties of Crystals: Their Representation by Tensors and Matrices* (Oxford science publications), reprinted. Oxford University Press, 1985, ISBN: 0198511655, 9780198511656.
- [17] S. Bian, R. Ossikovski, A. Canillas, G. Jellison, and O. Arteaga, "Spatial dispersion in silicon", *Phys. Rev. B*, vol. 109, p. 035 201, 3, 2024, DOI: 10.1103/PhysRevB.109.035201.
- [18] S. I. Pekar, "The Theory of Electromagnetic Waves in a Crystal in which Excitons Are Produced", *Journal of Experimental and Theoretical Physics*, vol. 6 (33), no. 4, p. 785, 1958, [Online]. Available: http://jetp.ras.ru/cgi-bin/e/index/e/6/4/p785?a=list.
- [19] R. M. A. Azzam and N. M. Bashara, *Ellipsometry and polarized light*. Amsterdam; New York: New York: North-Holland Pub. Co.; sole distributors for the U.S.A. and Canada, Elsevier North-Holland, 1977, ISBN: 9780720406948.
- [20] D. W. Berreman, "Optics in Stratified and Anisotropic Media: 4×4-Matrix Formulation", *J. Opt. Soc. Am.*, vol. 62, no. 4, pp. 502–510, 1972, doi: 10.1364/JOSA.62.000502.
- [21] P. Yeh, "Optics of anisotropic layered media: A new 4 × 4 matrix algebra", *Surface Science*, vol. 96, no. 1, pp. 41–53, 1980, ISSN: 0039-6028, DOI: https://doi.org/10.1016/0039-6028(80)90293-9.
- [22] F. I. Fedorov, "The Theory of the Optical Activity of Crystals", Soviet Physics Uspekhi, vol. 15, no. 6, p. 849, 1973, doi: 10.1070/PU1973v015n06ABEH005099.
- [23] D. Franta, P. Franta, J. Vohánka, M. Čermák, and I. Ohlídal, "Determination of thicknesses and temperatures of crystalline silicon wafers from optical measurements in the far infrared region", *Journal of Applied Physics*, vol. 123, no. 18, p. 185707, 2018, ISSN: 0021-8979, DOI: 10.1063/1.5026195.
- [24] D. Franta, J. Vohánka, and B. Hroncová, "Dispersion models exhibiting natural optical activity: theory of the dielectric response of isotropic systems", *J. Opt. Soc. Am. B*, vol. 40, no. 11, pp. 2928–2941, 2023, DOI: 10.1364/JOSAB.497572.
- [25] B. Hroncová, "Characterization of optically active liquids", Bachelor's thesis, Brno, 2022, [Online]. Available: https://is.muni.cz/th/b8d9r/.
- [26] D. Franta, D. Nečas, L. Zajíčková, and I. Ohlídal, "Broadening of dielectric response and sum rule conservation", *Thin Solid Films*, vol. 571, pp. 496–501, 2014, doi: 10.1016/j.tsf.2013.11.148.

- [27] S. Nichols, O. Arteaga, A. Martin, and B. Kahr, "Measurement of transmission and reflection from a thick anisotropic crystal modeled by a sum of incoherent partial waves", *J. Opt. Soc. Am. A*, vol. 32, no. 11, pp. 2049–2057, 2015, DOI: 10. 1364/JOSAA.32.002049.
- [28] K. Postava, T. Yamaguchi, and R. Kantor, "Matrix description of coherent and incoherent light reflection and transmission by anisotropic multilayer structures", *Appl. Opt.*, vol. 41, no. 13, pp. 2521–2531, 2002, DOI: 10.1364/A0.41.002521.
- [29] A. T. Martin, S. M. Nichols, M. Tan, and B. Kahr, "Mueller matrix modeling of thick anisotropic crystals with metallic coatings", *Applied Surface Science*, vol. 421, pp. 578–584, 2017, 7th International Conference on Spectroscopic Ellipsometry, ISSN: 0169-4332, DOI: https://doi.org/10.1016/j.apsusc.2016.10.124.
- [30] R. C. Jones, "A New Calculus for the Treatment of Optical Systems V. A More General Formulation, and Description of Another Calculus", *J. Opt. Soc. Am.*, vol. 37, no. 2, pp. 107–110, 1947, doi: 10.1364/JOSA.37.000107.
- [31] I. Ohlídal, J. Vohánka, M. Čermák, and D. Franta, "Optical Characterization of Thin Solid Films", in Springer Cham, 2018, ch. 9, 233–267, ISBN: 978-3-319-75324-9, DOI: 10.1007/978-3-319-75325-6\_9.
- [32] R. C. Jones, "A New Calculus for the Treatment of Optical Systems. VII. Properties of the N-Matrices", J. Opt. Soc. Am., vol. 38, no. 8, pp. 671–685, 1948, DOI: 10.1364/JOSA.38.000671.
- [33] R. M. A. Azzam, "Propagation of partially polarized light through anisotropic media with or without depolarization: A differential 4 × 4 matrix calculus", *J. Opt. Soc. Am.*, vol. 68, no. 12, pp. 1756–1767, 1978, DOI: 10.1364/JOSA.68.001756.
- [34] O. Arteaga, "Useful Mueller matrix symmetries for ellipsometry", *Thin Solid Films*, vol. 571, pp. 584–588, 2014, 6th International Conference on Spectroscopic Ellipsometry (ICSE-VI), ISSN: 0040-6090, DOI: https://doi.org/10.1016/j.tsf. 2013.10.101.
- [35] R. C. Jones, "New Calculus for the Treatment of Optical Systems. VIII. Electromagnetic Theory", *J. Opt. Soc. Am.*, vol. 46, no. 2, pp. 126–131, 1956, doi: 10.1364/JOSA.46.000126.
- [36] O. Arteaga, "Mueller matrix polarimetry of anisotropic chiral media", Doctoral dissertation, Barcelona, 2010, [Online]. Available: https://www.mmpolarimetry.com/phd-thesis/.
- [37] O. Arteaga, "Number of independent parameters in the Mueller matrix representation of homogeneous depolarizing media", *Opt. Lett.*, vol. 38, no. 7, pp. 1131–1133, 2013, DOI: 10.1364/OL.38.001131.
- [38] S. Bian, C. Cui, and O. Arteaga, "Mueller matrix ellipsometer based on discrete-angle rotating Fresnelrhomb compensators", *Appl. Opt.*, vol. 60, no. 16, pp. 4964–4971, 2021, DOI: 10.1364/A0.425899.

- [39] O. Arteaga, J. Freudenthal, B. Wang, and B. Kahr, "Mueller matrix polarimetry with four photoelastic modulators: theory and calibration", *Appl. Opt.*, vol. 51, no. 28, pp. 6805–6817, 2012, DOI: 10.1364/A0.51.006805.
- [40] J. Gomis-Brescó and O. Arteaga, "Use of complete temporal basis in polarimeters based on photoelastic modulators", *Opt. Lett.*, vol. 48, no. 7, pp. 1966–1969, 2023, poi: 10.1364/OL.487422.
- [41] H. H. Li, "Refractive index of alkaline earth halides and its wavelength and temperature derivatives", *Journal of Physical and Chemical Reference Data*, vol. 9, no. 1, pp. 161–290, 1980, ISSN: 0047-2689, DOI: 10.1063/1.555616.
- [42] D. Franta, J. Vohánka, D. Nečas, and P. Ondračka, "newAD2 optical characterization software", [Online]. Available: http://newad.physics.muni.cz/.
- [43] D. Franta, A. Dubroka, *et al.*, "Temperature-dependent dispersion model of float zone crystalline silicon", *Applied Surface Science*, vol. 421, pp. 405–419, 2017, 7th International Conference on Spectroscopic Ellipsometry, ISSN: 0169-4332, DOI: https://doi.org/10.1016/j.apsusc.2017.02.021.
- [44] I. J. A. Woollam Co., "Guide to Using WVASE®",